Coordination of actin plus-end dynamics by IQGAP1, formin, and capping protein

Morgan L. Pimm[1], Alexandra G. Marcin[1], Brian K. Haarer[1], Marcela Alcaide Eligio[1], and Jessica L. Henty-Ridilla[1,2,✉]

[1]Department of Biochemistry & Molecular Biology, SUNY Upstate Medical University, Syracuse, NY, 13210
[2]Department of Neuroscience & Physiology, SUNY Upstate Medical University, Syracuse, NY, 13210

Cell processes require precise regulation of actin polymerization at filament plus ends to execute normal functions. The detailed mechanisms used to control filament assembly at plus ends in the presence of diverse and often opposing regulators is not clear. Here we explore and identify residues important for the plus-end related activities of IQGAP1. In multi-wavelength TIRF assays, we directly visualize dimers of IQGAP1, mDia1, and CP on filament ends alone and as a multicomponent end binding complex. IQGAP1 promotes the turnover of end-binding proteins reducing the dwell times of CP, mDia1, or mDia1-CP 'decision complexes' by 8-18-fold. Loss of these activities in cells disrupts actin filament arrays, morphology, and migration. Together, our results reveal a role for IQGAP1 in promoting protein turnover on filament ends and provide new insights into how actin assembly is regulated in cells.

actin | IQGAP1 | formin | capping protein
Correspondence: ***ridillaj@upstate.edu***

Introduction

Actin filament assembly at the leading edge is highly regulated to produce filaments of specific length and structure to power diverse cell processes. Short filaments present in lamellipodia are regulated by high affinity interactions with plus ends and capping protein (CP) which block filament polymerization (Fujiwara et al., 2014; Funk et al., 2021; Wear et al., 2003). In contrast, long unbranched filaments present in filopodia or stress fibers are produced by plus end binding formin proteins, like mDia1 (Breitsprecher & Goode, 2013; Chesarone et al., 2010; Funk et al., 2021; Goode & Eck, 2007; Kovar et al., 2006; Rottner et al., 2017; Zweifel et al., 2021). Filament polymerization is further refined by complexes with formin to enhance (e.g., APC, CLIP-170, or spire) or with CP to limit (e.g., twinfilin or CARMIL) assembly (Bosch et al., 2007; Bradley et al., 2020; Breitsprecher et al., 2012; Hakala et al., 2021; Henty-Ridilla et al., 2016; Montaville et al., 2014; Mwangangi et al., 2021; Stark et al., 2017; Ulrichs et al., 2023; Wirshing et al., 2023). Remarkably, CP and mDia1 also form 'decision complexes' that pause filament assembly, until either protein leaves the plus end, reinitiating growth if CP dissociates first or extending the pause in growth if formin departs the first (Bombardier et al., 2015; Maufront et al., 2022; Shekhar et al., 2015).

IQ-motif containing GTPase activating protein 1 (IQGAP1) is a conserved 189 kDa scaffolding protein that coordinates actin and microtubule dynamics, cell signaling pathways, and other essential cell processes (Brandt et al., 2007; Brown & Sacks, 2006; Cao et al., 2015; Hedman et al., 2015; Shannon, 2012; White et al., 2012). IQGAP1 influences actin filaments in two ways: filament bundling via side-binding interactions, through an N-terminal calponin homology domain (CHD), and transient suppression of plus end growth via a 913 amino acid stretch of residues located in its C-terminus (744-1657)(Bashour et al., 1997; Hoeprich et al., 2022; J. Liu et al., 2016; Pelikan-Conchaudron et al., 2011; Ren et al., 2005). Notably, IQGAP1 is also a ligand of formins (i.e., mDia1 and INF2)(Bartolini et al., 2016; Brandt et al., 2007; Chen et al., 2020). Whether IQGAP1-formin activities influence actin assembly or multi-component plus-end regulatory systems like the formin-CP 'decision complex' is not known.

Here we identify the residues in IQGAP1 that mediate interactions with actin filament plus ends and that are required for transient filament capping. We examine the molecular interplay of IQGAP1 with the formin mDia1, CP, and the mDia1-CP decision complex at the plus end using single-molecule TIRF microscopy in four wavelengths. We show that IQGAP1 slows the mean rate of formin-assisted actin filament elongation. Further, IQGAP1 acts as a displacement factor freeing plus ends from mDia1, CP, or decision complexes. The loss of these activities disturbs cellular actin arrays, morphology, and migration. Overall, this strongly suggests IQGAP1 promotes more frequent exchange of proteins present on plus ends to regulate actin filament assembly.

Results

IQGAP1 bundles and transiently caps actin filament plus-ends.

We purified full length (FL)-IQGAP1 (Figure 1A) using two affinity systems and directly tested its effect on actin assembly in total internal reflection fluorescence (TIRF) microscopy assays (Figures 1B and S1A-C; Movies 1 and 2). Actin polymers in reactions containing IQGAP1 appeared sparse, short, and bundled compared to actin alone controls (Figures 1B and S1C). Most concentrations of IQGAP1 had no effect on actin nucleation ($P = 0.79$) (Figures 1C and S1D). In contrast, all IQGAP1 concentrations used significantly slowed actin filament elongation from 10.2 ± 0.2 (SE) subunits s^{-1} μM^{-1} to 6.7 ± 0.3 (SE) subunits s^{-1} μM^{-1} ($P < 0.0001$) (Figures 1D and S1E). A closer examination of filaments in reactions containing IQGAP1 revealed significantly more stochastic pauses in

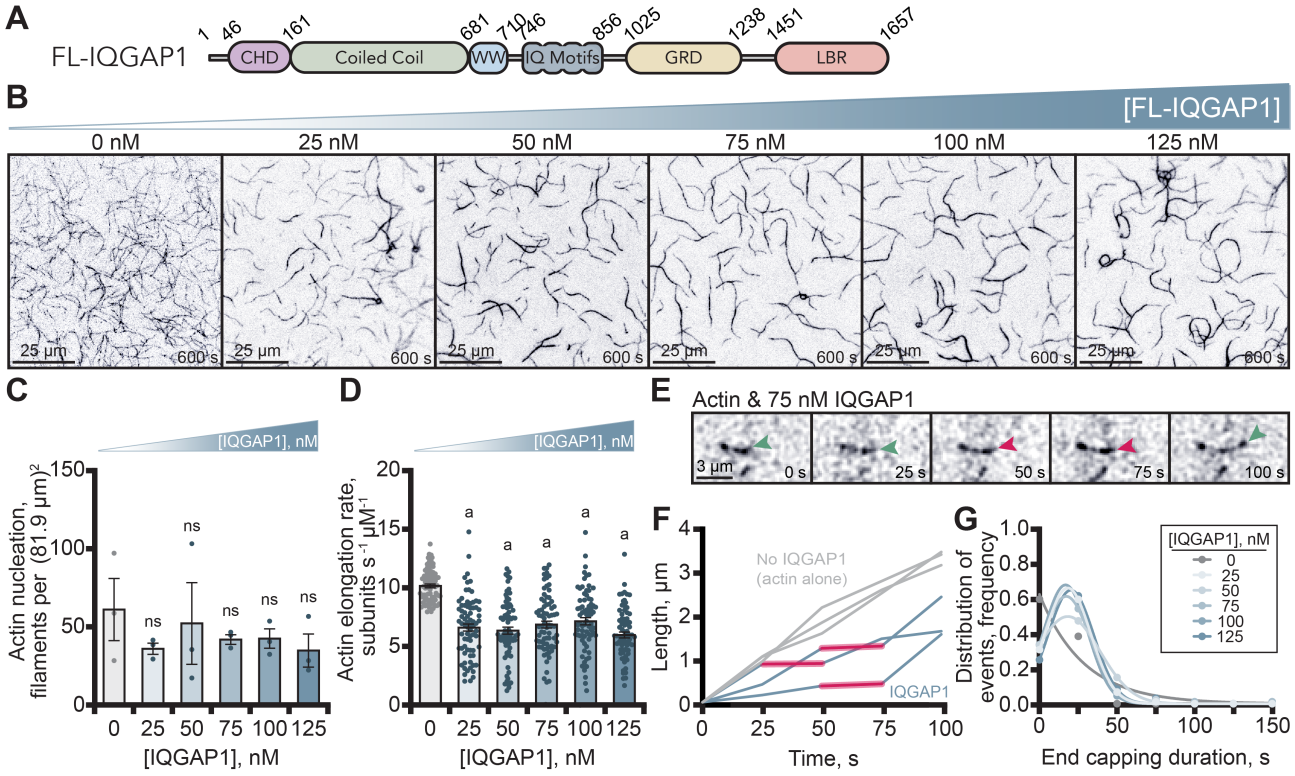

Figure 1. IQGAP1 caps the fast-growing ends of actin filaments. (A) Schematic of IQGAP1 domains. Abbreviations: CHD, calponin homology domain; WW, WW domain; GRD, GAP-related domain; LBR, ligand binding region. **(B)** Images from TIRF assays containing 1 µM actin monomers (20% Oregon Green(OG)-label) and concentrations of IQGAP1. Scale bars, 25 µm. **(C)** Actin filament nucleation 200 s after initiation from reactions in B (n = 3 fields of view). Error bars indicate SE. Statistics, ANOVA: a, significantly different from control (No IQGAP1); ns, not different from control. **(D)** Actin filament elongation rates from TIRF reactions in B (n = 75 filaments per condition; pooled from 3 different trials). Statistics as in C. **(E)** Example actin filament that exhibits a pause in growth (red arrows). Scale bar, 3 µm. **(F)** Example length over time plots from reactions containing actin (grey) or actin and 75 nM IQGAP1 (teal). Red shading indicates the duration of filament pausing events. **(G)** Frequency distribution plots of the duration of IQGAP1 capping events from reactions measured in D (n = 75 filaments, and 31-70 pause events per condition, 331 pauses total measured). The mean duration of individual capping events was 20.6 s in the presence of IQGAP1 (regardless of concentration).

plus-end growth, lasting an average of 20.6 ± 1.9 (SE) s, regardless of concentration (Figures 1E-G and S1F-I; Movie 3). Greater than 70% of all filaments polymerized with IQGAP1 displayed capping events (Figures 1F and S1F, S1H-I). Thus, IQGAP1 slows actin polymerization by transiently capping filament plus-ends (Hoeprich et al., 2022; Pelikan-Conchaudron et al., 2011). Notably, IQGAP1 purified by GST-affinity displayed dose-dependent changes in nucleation and plus-end dwell time (Figure S1D, S1G, and S1I), which may indicate an effect of the GST-tag on IQGAP1 function. All further analyses were performed with proteins purified by His-affinity.

IQGAP1(CD) abrogates filament capping activity.

The plus-end capping activity of IQGAP1 is associated with residues 745-1502 (Hoeprich et al., 2022; Pelikan-Conchaudron et al., 2011). We used truncation and mutational analyses with 75 nM protein to further delimit the region and residues important for plus end capping because it is sufficient for plus-end binding (k_D = 25-35 nM)(Hoeprich et al., 2022; Pelikan-Conchaudron et al., 2011) and filament pauses were obvious with the full-length protein (Figures 1E, 2A, and S2A-G; Movies 4 and 5). IQGAP1(745-1024), containing four IQ motifs and the predicted dimerization domain, was the smallest truncation able to cap actin filaments (Figures 2A-C and S2). As this fragment was prone to degradation, we explored the contribution of each IQ motif with structurally disruptive mutations in IQGAP1(745-1450). All truncated IQGAP1 proteins that contained residues C756 and C781 capped filaments (Figures 2A, 2C, and S2A-D). We generated alanine substitution mutants for these residues in IQGAP1(745-1450) and in the full-length protein. The elongation rate of actin filaments polymerized in the presence of the truncated or full-length substitution mutant was equivalent to controls lacking IQGAP1 (7.0 ± 0.1 (SE) subunits s^{-1} μM^{-1} compared to 7.6 ± 0.1 subunits s^{-1} μM^{-1})(P = 0.70), and significantly faster than reactions performed with FL-IQGAP1 (5.8 ± 0.1 subunits s^{-1} μM^{-1})(P < 0.0001), indicating these mutations abolish IQGAP1-mediated filament capping. Further, length traces of actin filaments polymerized with either capping-deficient (CD) IQGAP1 displayed uninterrupted polymerization (Figures 2D and S2B) and pauses to filament growth indistinguishable from reactions that contain only uncapped filaments lacking IQGAP1 (Figures 2E and S2B-G) (P > 0.99).

IQGAP1(CD) is a dimer that does not bind plus-ends.

IQGAP1(CD) appears to lack capping activity (Figure 2 and S2). However, measuring this activity from single-color actin assays does not rule out potential mechanisms

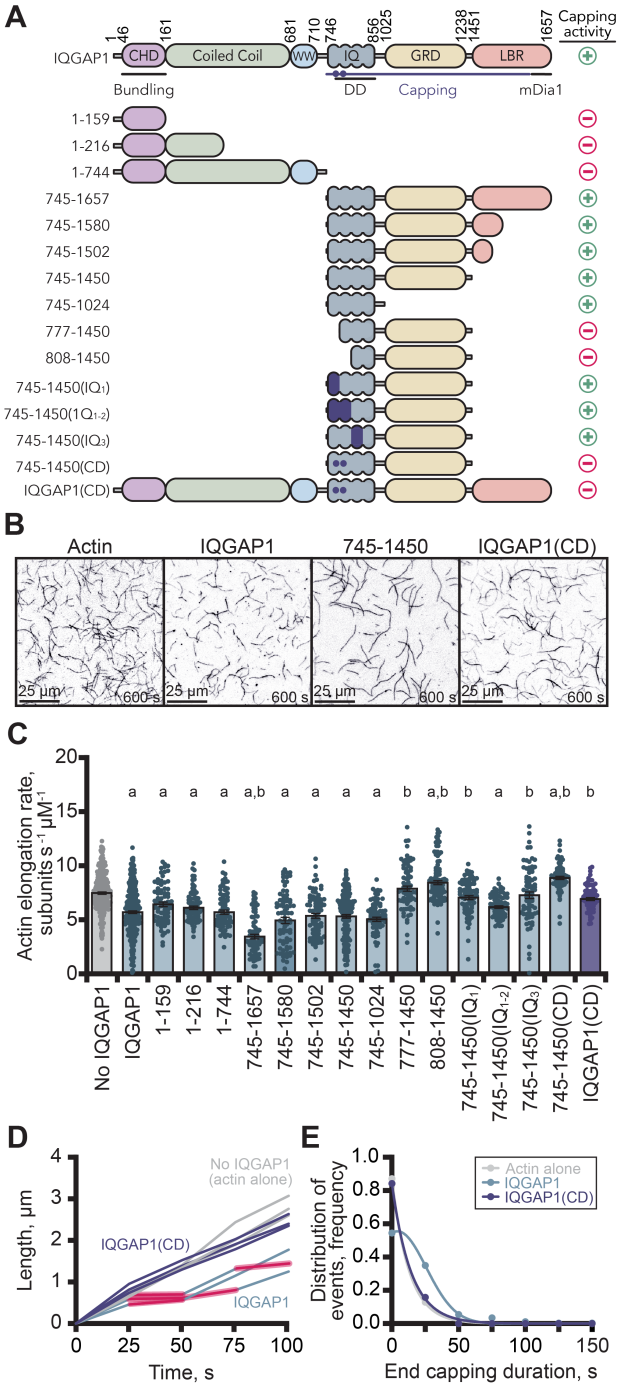

Figure 2. IQGAP1(CD) abrogates filament capping. (A) IQGAP1 constructs that cap (+) and fail to cap (–) actin filaments. Specific functional regions and formin (mDia1) binding area are highlighted. DD, dimerization domain. Purple dots, two residues necessary for capping activity. **(B)** TIRF images from assays containing 1 µM actin (20% OG-label) or actin and 75 nM IQGAP1 proteins. CD, capping deficient. Scale bars, 25 µm. **(C)** Actin filament elongation rates from B (n = 75-324 filaments per condition; pooled from at least 3 different experiments). Error bars indicate SE. Statistics, ANOVA: a, significantly different from actin; b, significantly different from actin and 75 nM FL-IQGAP1. IQGAP1(CD) does not cap actin filaments shown by **(D)** filament length traces and **(E)** frequency plots of the duration of IQGAP1-mediated pauses (n = 75 filaments per condition; n = 159 pauses for IQGAP1; n = 12 for IQGAP1(CD)).

where the alanine substitutions disrupt IQGAP1 oligomerization. To address this, we generated fluorescently labeled SNAP-tagged versions of IQGAP1 and IQGAP1(CD) and used step-photobleaching analysis to determine the oligomeric state of single molecules of 649-IQGAP1 or 488-IQGAP1(CD) each predominately exist as dimers (Figure 3A-C). In multi-wavelength TIRF assays with polymerizing actin filaments, 649-IQGAP1 molecules localized to filament plus-ends of actin filaments, as expected (Figure 3D; Movie 6). However, the mean elongation rate of actin filaments actin filaments these reactions was significantly slower at 3.1 ± 0.3 (SE) subunits s^{-1} μM^{-1}, compared to actin alone controls (P<0.0001), likely due to the direct visualization of end-localization events (Figure 3D-F)(Hoeprich et al., 2022). In contrast, 488-IQGAP1(CD) protein showed rare interactions with filament ends (Figure 3D and 3G) and elongated at rates comparable to the actin alone control (Figure 3E-F) (P = 0.81). Molecules of either 649-IQGAP1 or 488-IQGAP1(CD) were observed on the sides of actin filaments (Figure 3H) and each labeled construct displayed filament bundling activities (Figure 3I).

IQGAP1 and mDia1(ΔDAD) form complexes that pause actin filament elongation.

IQGAP1 directly binds the formin, mDia1, which nucleates and processively elongates actin filaments (Figures 4A and S3A)(Brandt et al., 2007; Chen et al., 2020). Biochemical evidence suggests these proteins may function antagonistically or influence additional actin filament end binding proteins that regulate filament assembly, like the formin-capping protein 'decision complex' (Bombardier et al., 2015; Funk et al., 2021; Hoeprich et al., 2022; Shekhar et al., 2015). We used TIRF microscopy assays to evaluate whether IQGAP1-formin complexes bound to filament ends and to address related consequences for actin polymerization. We purified two constitutively active versions of fluorescently labeled formin, 549-mDia1(ΔDAD), which retains the IQGAP1 binding site, and 549-mDia1(FH1-C), which does not (Brandt et al., 2007; Chen et al., 2020). Single-molecule assays that contained 549-mDia1(ΔDAD) showed significantly more colocalization with either 649-IQGAP1 or 488-IQGAP1(CD), compared to 549-mDia1(FH1-C) (Figure 4B and 4C), as expected. Molecules of 549-mDia1(ΔDAD) processively tracked the plus-ends of actin filaments (Figure 4D)(Breitsprecher et al., 2012; Kovar et al., 2006). We also observed the formation and dissolution of mDia1(ΔDAD)-IQGAP1 complexes at filament plus-ends (Figure 4D-E and S3B-D; Movie 7), albeit rarely for 488-IQGAP1(CD) and likely mediated by formin (Figure 4D). In the example shown (Figure 4E), the actin filament grew at an average rate of ~10 subunits s^{-1} μM^{-1}, consistent with unassisted actin filament assembly (Kovar et al., 2006; Kuhn & Pollard, 2005; Liu et al., 2022; Pimm et al., 2022). Upon association of a pre-formed mDia1-IQGAP1 complex, filament growth stalled, with most pauses occurring for an average of 19.9 ± 2.4 s (Figure S3E), despite the example shown. Eventually the complex dissociates and a molecule

of 549-mDia1(ΔDAD) rejoins the filament, growing 36.7 subunits s^{-1} μM^{-1}, consistent with formin-based filament assembly (Breitsprecher et al., 2012; Henty-Ridilla et al., 2016; Kovar et al., 2006; Vizcarra et al., 2014). Notably, stochastic pauses in formin-mediated actin filament growth occurred only when IQGAP1 could directly bind formin i.e., 549-mDia1(ΔDAD), and were rarely observed for reactions performed with 549-mDia1(FH1-C) or IQGAP1(CD) (Figure 4D-G).

IQGAP1 influences 'decision complexes' by promoting dynamic exchange of plus-end molecules.

IQGAP1, mDia1, and additional proteins competitively regulate actin filament plus-ends and produce vastly different consequences for filament length, assembly dynamics, and array architecture (Courtemanche, 2018; Romet-Lemonne & Jégou, 2021; Shekhar et al., 2016). For example, mDia1 participates in an epic 'tug-of-war' with capping protein (CP) to decide the polymerization fate of individual actin filaments. The formin 'wins' when filament growth resumes (CP dissociates), whereas formin 'loses' when CP evicts it from the plus-end resulting in no additional growth (Bombardier et al., 2015). To address whether IQGAP1 influenced mDia1-CP 'decision complexes' we performed bi-color actin TIRF assays (Figure 5A). Actin filaments present in reactions containing buffer controls and capping-deficient IQGAP1(CD) are predominately two colors, indicating that plus-ends are unobstructed (Figures 5B-C and S4A; Movie 8). In contrast, actin filaments in reactions containing CP had a significantly higher percent of filaments that remained the original color (pink) ($P < 0.0001$), indicating capping events blocked the site of new monomer addition (Figures 5B-C and S4A; Movie 8). The varied length of bi-color filaments present in the IQGAP1 reactions suggests that brief capping events occur (Figures 5B and S4A). These reactions had more blocked ends than buffer controls ($P = 0.0002$), but significantly more free ends compared to reactions containing CP ($P = 0.003$) (Figure 5C). Consistent with our single filament analysis, significantly more ends were blocked with the combination of IQGAP1 and mDia1(ΔDAD) ($P = 0.0132$) (Figures 4F, 5D-E, and S4B; Movie 8). Assays assessing the mDia1(ΔDAD)-CP 'decision complex' displayed predominately blocked filament ends compared to actin alone controls ($P < 0.0001$) or reactions containing CP alone ($P = 0.79$) (Figures 5F-G and S4C; Movie 8). Remarkably, the addition of IQGAP1 to either condition resulted in significantly fewer blocked ends ($P < 0.0001$), although significantly fewer free-ends compared to buffer controls ($P = 0.897$) (Figures 5F-G and S4C; Movie 8).

To better understand how the combination of two capping factors (e.g., IQGAP1 and CP) resulted in more free-ends, we turned to four-color single-molecule TIRF microscopy, directly visualizing non polymerizing actin filaments, IQGAP1, mDia1(ΔDAD), and CP at different fluorescent wavelengths (Figure 6A-B' Movie 9). We observed and measured the lifetime of individual molecules alone or any com-

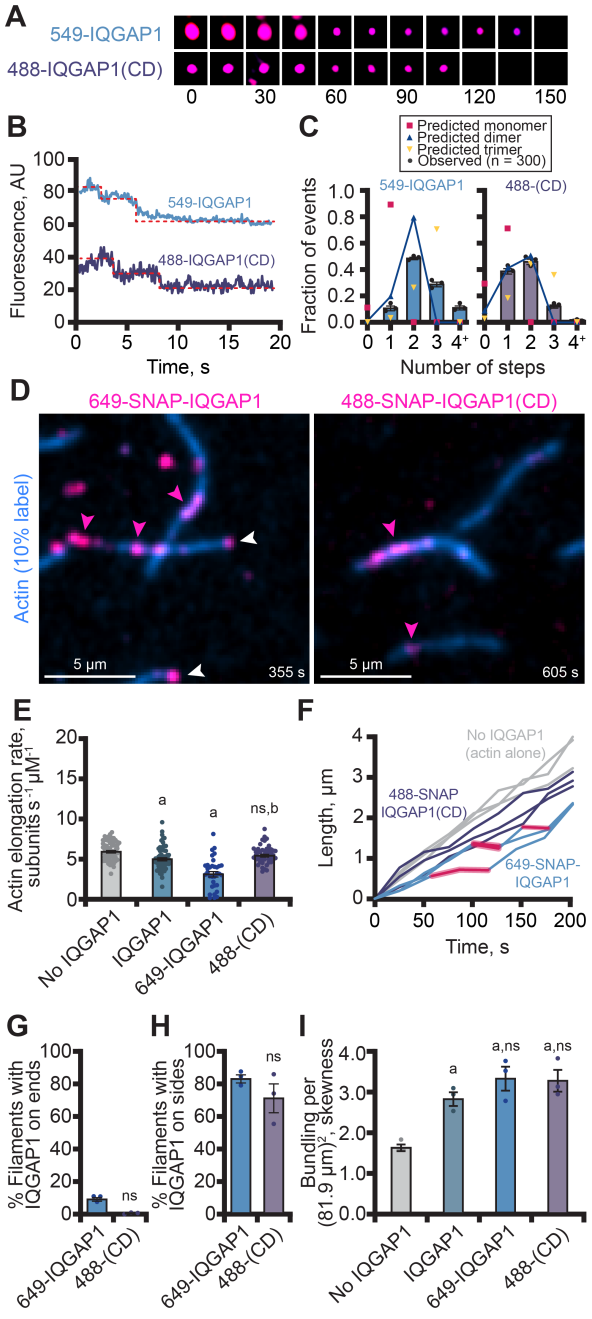

Figure 3. IQGAP1(CD) is a dimer that does not cap actin filaments. **(A)** Single-molecules of labeled IQGAP1 or IQGAP1(CD) subjected to step-photobleaching. **(B)** Fluorescence intensity profiles of representative step photobleaching events for 5 nM SNAP-IQGAP1 proteins as imaged in A. Red lines emphasize photobleaching steps. **(C)** Fluorescence intensity predictions and analysis of SNAP-IQGAP1 molecules (n = 300 molecules per protein, pooled from 3 experiments) as in D-E. **(D)** Two-color TIRF images showing the localization of 649-IQGAP1 or 488-IQGAP1(CD). Reactions contain: 1 µM actin (10% 488- or 647-Alexa label) and 5 nM SNAP-IQGAP1 construct. Arrows depict filament end- or side-binding events. Scale bars, 5 µm. **(E)** Actin filament elongation rates comparing actin alone control with 5 nM untagged or 5 nM SNAP-tagged versions of IQGAP1. Conditions as in A (n = 33-75 filaments (dots) per condition pooled from 3 independent experiments). Error bars indicate SE. Statistics, ANOVA: a, significantly different from no IQGAP1 control; b, significantly different from actin and untagged IQGAP1; ns, not different from control. **(F)** Representative length traces of filaments from reactions in B. Red shading indicates the duration of filament capping events. **(G)** Percent of all actin filaments with labeled-IQGAP1 molecules present on the plus-end (n = 73-144 filaments per field of view, 335-372 measured total). **(H)** Percent of actin filaments from G with side bound IQGAP1 molecules. **(I)** Actin filament bundling was quantified at 1200 s from TIRF fields described in B, with skewness parameter (n = 3 fields of view per condition).

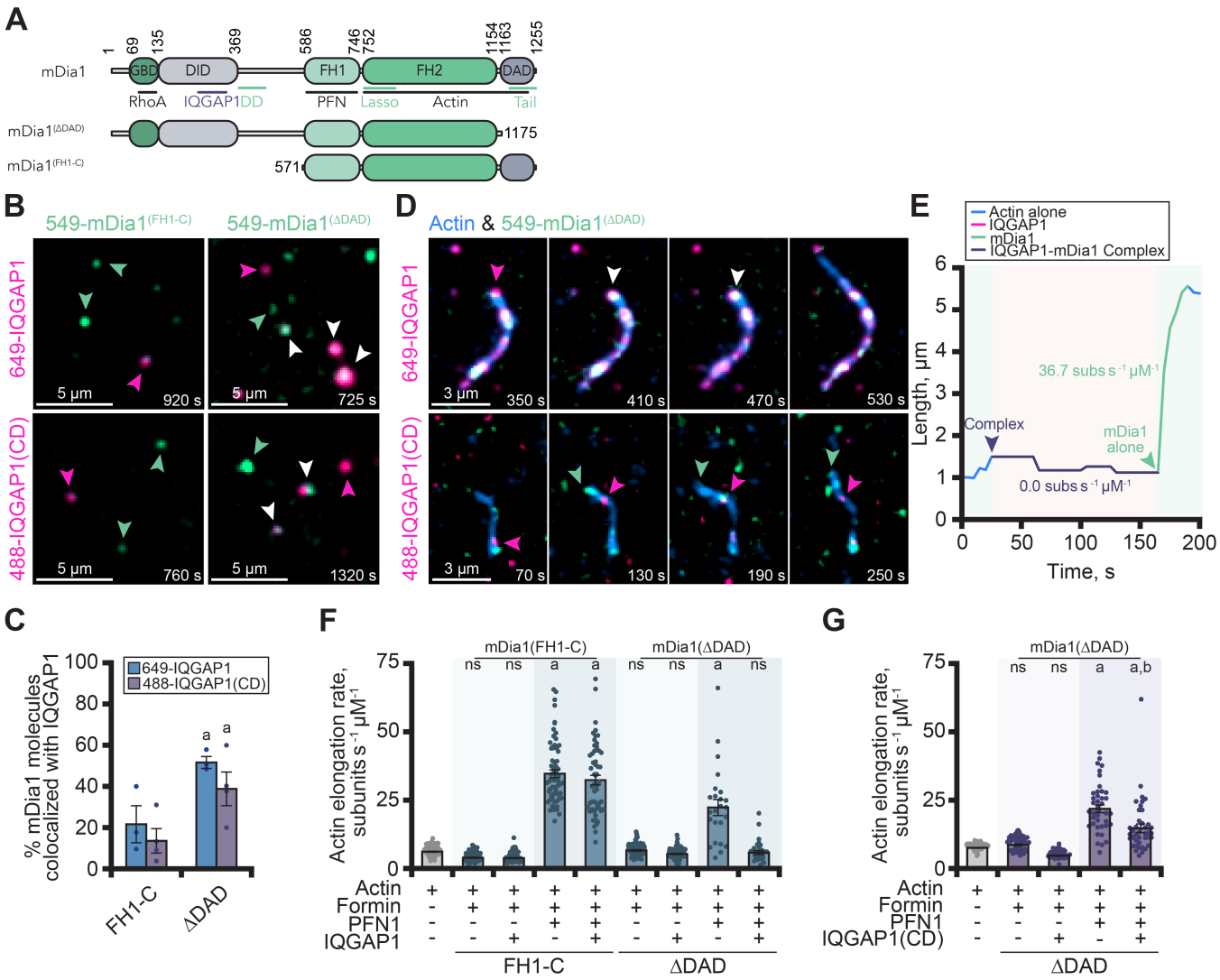

Figure 4. IQGAP1 and formin co-occupy plus-ends and pause filament elongation. **(A)** Schematic of formin (mDia1) constructs that do not bind (FH1-C) or bind (ΔDAD) to IQGAP1. Abbreviations: GBD, GTPase-binding domain; DID, Diaphanous inhibitory domain; FH1, formin homology region 1; FH2, formin homology 2 domain; DAD, Diaphanous autoregulatory domain. Structural features of mDia1 are labeled with green lines. DD, dimerization domain. **(B)** Single molecule colocalization of 10 nM 549-mDia1 constructs with 10 nM 649-IQGAP1 or 10 nM 488-IQGAP1(CD) by TIRF. Arrows highlight examples of SNAP-IQGAP1 (pink), SNAP-mDia1 (green) or colocalized molecules (white). Scale bars, 5 μm. **(C)** Colocalization of formin-IQGAP1 complexes as in B. Error bars indicate SE. Dots are individual values for n = 3-4 replicates. Statistics, ANOVA: a, significantly more association compared to mDia1(FH1-C). **(D)** Triple-color TIRF of actin filaments (blue; 10% 488- or 647-Alexa label) polymerizing in the presence of 5 μM profilin, 10 nM 549-mDia1(ΔDAD) (green), and 10 nM 649-IQGAP1 or 488-IQGAP1(CD) (pink). Arrows as in B. Scale bars, 3 μm. **(E)** Elongation rates correlate with arrival and dissociation of 649-IQGAP1 or mDia1(ΔDAD) at the barbed end. **(F)** Effects of IQGAP1 on the rate of mDia1-mediated actin filament elongation. Reactions as in D with unlabeled proteins. **(G)** Effects of IQGAP1(CD) on the rate of mDia1-mediated elongation. Reactions as described in D. Error bars in F-G indicate SE. Dots in F-G represent individual filaments measured (n = 24-105 per condition, pooled from at least 3 independent trials). Statistics as in C: a, different from actin alone and formin controls lacking profilin; b, different from reactions containing formin and profilin.

plexes associated with filament ends. The half-life and behavior of individual molecules of 649-IQGAP1 (n = 17), 488-mDia1(ΔDAD) (n = 14), or 549-CP (n = 2) or mDia1-CP decision complexes (n = 20) on filament ends was consistent with previous studies (Figures 6C-D and S4D). We observed several IQGAP1-CP complexes (n = 7) that were displaced from plus-ends 8-fold faster than individual molecules of CP alone (Figures 6 and S4D). We also visualized several very short-lived (~27 s) IQGAP1-mDia1-CP complexes (n = 21) on plus-ends (Figure S4D). Both the dwell time and half-life of these IQGAP1-mDia1-CP complexes were similar to the time that individual molecules of IQGAP1 were present on plus-ends, but drastically reduced compared to any combination of CP or formin (Figures 6D and S4D). Thus, not only does IQGAP1 transiently cap actin filaments, it also competitively displaces longer-lived decision complexes and individual plus-end regulators >18-fold!

IQGAP1 capping activities are required for cell morphology and migration.

Normal cell morphology and migration depends on IQGAP1 (Brandt et al., 2007; Choi et al., 2013; Fukata et al., 1997). Thus, to test the importance of these activities in a more physiological setting, we generated two IQGAP1 CRISPR knock-out lines in NIH 3T3 cells (Figure S5A). Loss of IQGAP1 significantly altered the morphology of these cells

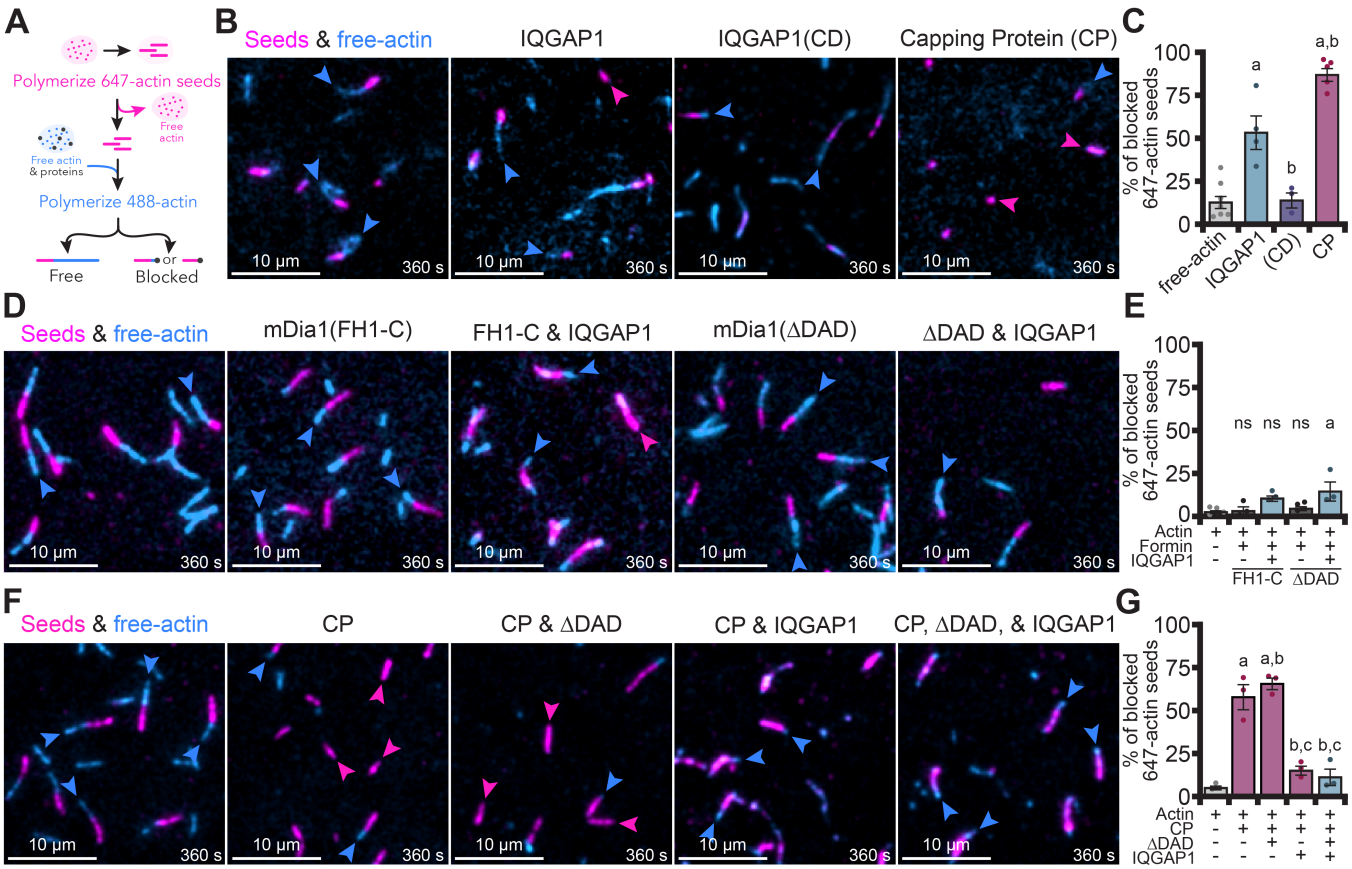

Figure 5. IQGAP1 protects filament ends from Capping Protein (CP). (A) Schematic of approach. Pink filament seeds with available ends will become bicolor filaments upon addition of blue actin monomers (free ends) or remain pink (blocked/capped ends). **(B)** Two-color actin filament assay visualized by TIRF. Reactions contain biotinylated 647-actin filament "seeds" polymerized for 2-3 mins before the reaction volume is replaced with 0.5 µM free-actin monomers (20% OG (top row only) or 10% 488-Alexa label) and buffer (control), 250 nM IQGAP1, 250 nM IQGAP1(CD), or 10 nM CP. **(C)** Quantification of blocked ends from reactions in B. Statistics, ANOVA: a, significantly different from control; b, significantly different from reactions containing IQGAP1. **(D)** Reactions performed as in B with the following conditions: buffer or 10 nM mDia1 protein, or 250 nM IQGAP1. **(E)** Quantification and statistics as in C for reactions in D. **(F)** Reactions performed as in B and D in the following combinations: buffer, CP, CP and mDia1(ΔDAD), CP and IQGAP1, or CP, mDia1(ΔDAD), and IQGAP1. All scale bars, 10 µm. **(G)** Quantification and statistics as in C for reactions in F.

(P=0.0142) and resulted in the loss of tension-sensitive stress-fibers (Figure 7A-D) (Senger et al., 2019). These knockout phenotypes were rescued with a plasmid expressing a full-length Halo-IQGAP1 construct (P = 0.0449), but not the Halo-IQGAP1(CD) mutant (P = 0.9999), compared to Halo-IQGAP1) (Figure 7A-D). The loss of IQGAP1 also significantly reduced cell migration in wound healing assays (P < 0.0001) (Figure 7E-F). Migration could be restored with Halo-IQGAP1 (P = 0.0004), albeit with some negative effects to cell-adhesion, but not with Halo-IQGAP1(CD) (P = 0.1199, compared to Halo-IQGAP1) (Figure 7E-F). These conditions did not significantly alter microtubule arrays (Figure S5D-E), which suggests these phenotypes may be specific to actin-based IQGAP1 functions. Thus, IQGAP1 plus-end activities govern the actin dynamics required to regulate cell shape and movement.

Discussion

Actin polymerization is regulated by vastly different and often opposing classes of plus-end binding proteins and protein-protein complexes that stimulate, arrest, or pause filament growth. This feature has remarkable consequences for cellular processes and behaviors, as plus-end protein processivity dictates the physical properties and structural dimensions of cellular actin arrays (Bombardier et al., 2015; Breitsprecher & Goode, 2013; Efimova et al., 2020; Funk et al., 2021; Henty-Ridilla et al., 2016; Hoeprich et al., 2022; Shekhar et al., 2015; Ulrichs et al., 2023; Wirshing et al., 2023). Filament assembly is further complicated by disassembly factors and other proteins that effectively limit available monomers necessary to assemble more filaments (Pimm et al., 2020; Pollard, 2016; Skruber et al., 2018). How this actin assembly paradox is resolved in cells remains unclear. Here we examine the role of IQGAP1 in actin filament assembly and identify two amino acids that are necessary for plus-end related activities. Our results suggest IQGAP1 is a displacement factor that rapidly exchanges formin, capping protein (CP), and formin-CP complexes, which may promote more transitions of different plus-end proteins (Figure 7G). This idea is reinforced in cells where IQGAP1 interactions with actin filament plus-ends are required for proper morphology and migration. Thus, IQGAP1 is part of a mechanism that may explain why cells require opposing and redundant factors to execute actin functions.

Individual molecules of the formin mDia1 or CP each exhibit high affinity (<1 nM), long lived (> 2000 s) interactions

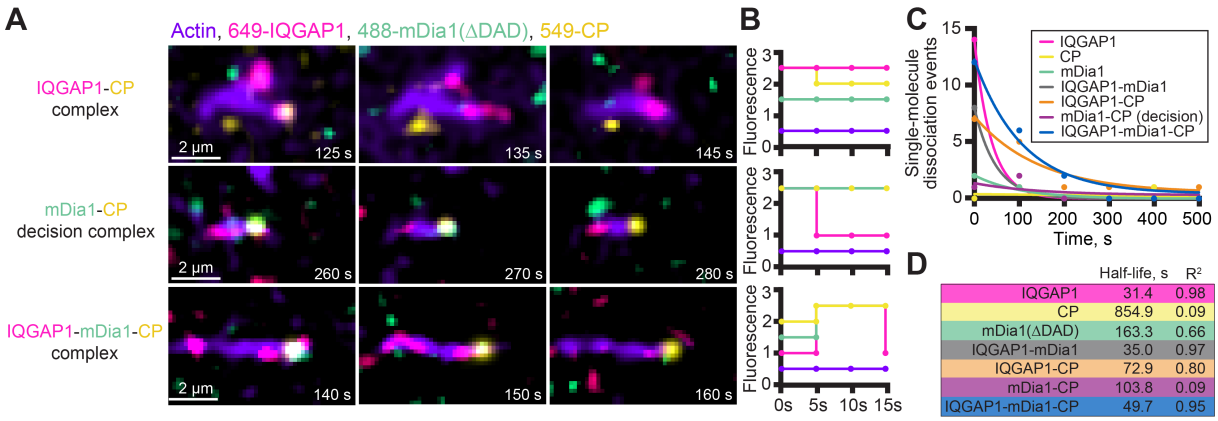

Figure 6. Single-molecules of IQGAP1 promote the dynamic exchange of plus-end factors. (A) Four-color TIRF microscopy images of plus-end complexes. Reactions contain: 1 μM actin (30% 405-Alexa label), 10 nM 488-mDia1(ΔDAD), 10 nM 549-CP, and 10 nM 649-IQGAP1. Scale bars, 2 μm. **(B)** Fluorescence intensity for examples in (A) showing the formation or dissolution of plus-end complexes. **(C)** Dissociation of single molecules and complexes from actin filament plus-ends. **(D)** The plus-end half-life of each complex determined in C.

with actin filament plus ends (Bombardier et al., 2015; Fujiwara et al., 2014; Funk et al., 2021; Shekhar et al., 2015). As a 'decision complex', mDia1-CP has shorter interactions with filament plus ends (493 s). These dynamic interactions allow for quick transitions between periods of growth or filament capping, to control actin filament length in actin-based structures like filopodia, stereocilia, or sarcomeres. IQGAP1 and mDia1 are high affinity binding partners with similar features to decision complexes (Bartolini et al., 2016; Brandt et al., 2007; Chen et al., 2020; Gaillard et al., 2011). Here we used formin mutants to show that both IQGAP1 and mDia1 can co-exist on filament plus-ends without binding each other or affecting formin-based activities. However, in situations where IQGAP1 was able to bind both mDia1 and filament plus-ends, the average formin-mediated assembly rate was reduced. However, unlike decision complexes, we never directly visualized molecules of mDia1 binding to filament ends before IQGAP1. Indeed, mDia1 joined IQGAP1 molecules already present on the plus end or IQGAP1-mDia1 joined as a preformed complex. Based on affinities alone, it is unlikely IQGAP1 outcompetes mDia1 for these ends, but perhaps side-binding or sliding interactions (below our detection limit) keep IQGAP1 molecules near filament ends (Bombardier et al., 2015; Maufront et al., 2022). With 4-color single-molecule assays we observed IQGAP1-mDia1-CP complexes on plus ends for an average of 27 s—18-fold less than mDia1-CP complexes. While the decision complex is a molecular "duel" or "tug-of-war" between mDia1 and CP, IQGAP1 seems to be a "decision factor" that determines the outcome by booting competitors off the plus end, effectively clearing the stage for the next battle.

Previous studies characterized IQGAP1 as a transient capping factor (Hoeprich et al., 2022; Pelikan-Conchaudron et al., 2011). Here we classify it as a displacement factor. In either situation, are these plus-end activities relevant in cells? IQGAP1 is localized to sites of meticulous actin filament end regulation including filopodia (Jacquemet et al., 2019), along stress fibers (Samson et al., 2017), and at the leading edge (Brandt et al., 2007; Chen et al., 2020). The highest concentration of filament ends exists in the lamellipodium, which has an estimated 500 actin filaments per μm squared (Abraham et al., 1999; Raz-Ben Aroush et al., 2017; Svitkina et al., 1997). Absent of plus-end factors, there would be 1,720-5,000 free ends in an average lamellipodium (1 μm × 10 μm × 0.2 μm) (Abraham et al., 1999; Raz-Ben Aroush et al., 2017; Svitkina et al., 1997). If we consider plus-end factors (and assume they are all active), 1,200 ends will be occupied by CP (1 μM)(Pollard & Borisy, 2003), <60 ends will be occupied by mDia1 dimers (<100 nM)(Chhabra et al., 2009), leaving as few as 460 free ends that could be occupied by 243 dimers of IQGAP1. Considering IQGAP1 side-binding affinity (47 μM)(Mateer et al., 2004) and other regulators that also bind these proteins, like twinfilin (602 molecules in this space)(Johnston et al., 2018) or other formins like INF2 (180 dimers)(Chhabra et al., 2009), there may not be enough free ends to bind all the regulators. However, evidence indicates that multiple regulators co-occupy filament plus-ends and our work suggests that IQGAP1 indiscriminately joins several factors present there (Brown & Sacks, 2006; Hedman et al., 2015; White et al., 2012). This may explain how the IQGAP1(CD) substitution mutant displayed significant perturbation to actin-based cell processes. Specifically, cells may not migrate as efficiently because formin-engaged filaments are overgrowing, and CP-subdued ends are being capped for too long. Intriguingly, IQGAP1 activities in cells are further regulated by calmodulin (CaM) and one of the two residues necessary for plus-end activities (C756) is present at the predicted binding site (Pelikan-Conchaudron et al., 2011; Zhang et al., 2019). Unraveling these molecular details provides a foundation for future studies to examine how additional plus-end regulators and IQGAP1 ligands further influence actin filament assembly.

Methods

Reagents.

All chemicals were obtained from ThermoFisher Scientific (Waltham, MA), unless otherwise stated. Synthesis

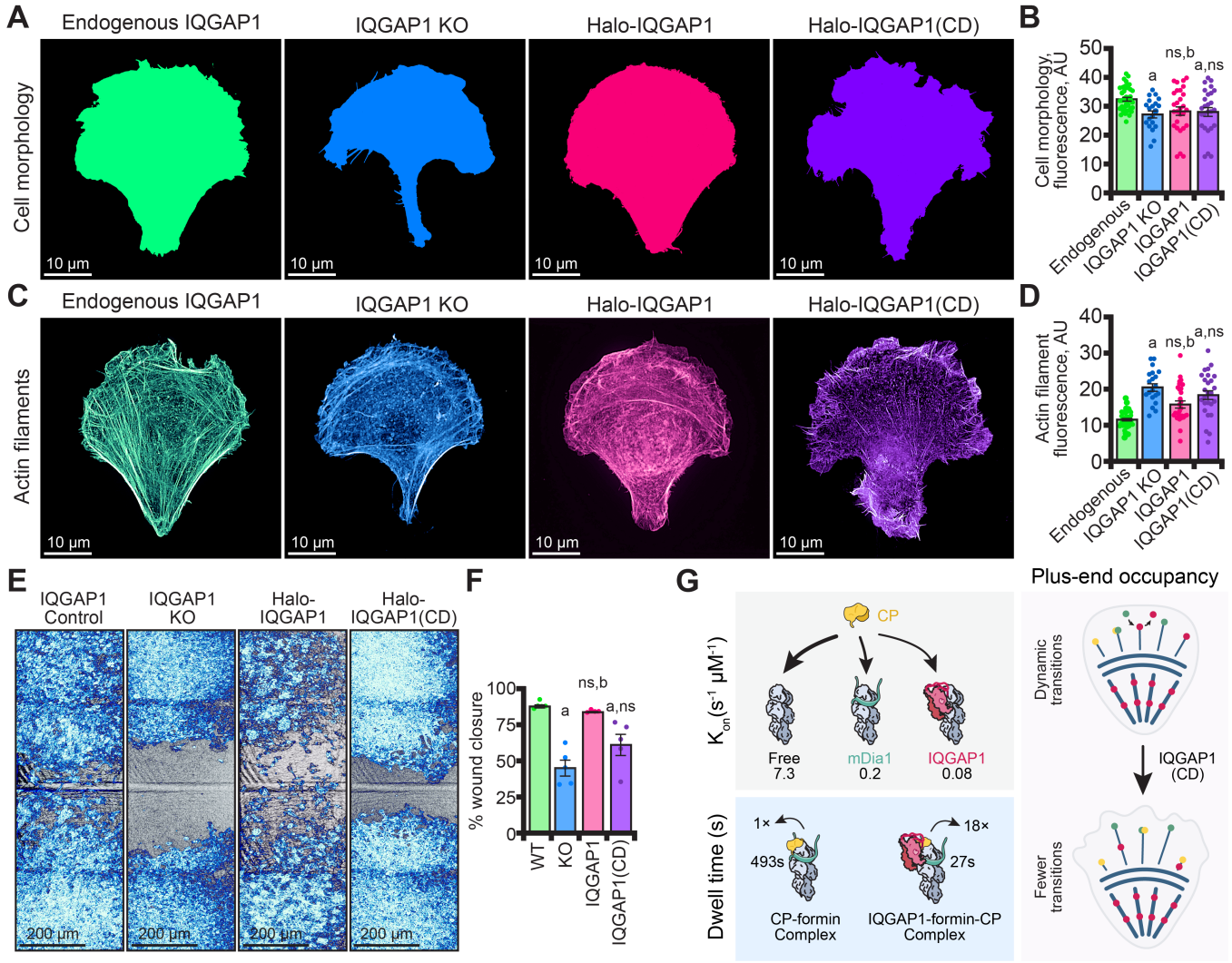

Figure 7. IQGAP1-mediated actin filament capping events influence the morphology and migration of NIH-3T3 cells. **(A)** Representative cell morphology of 3T3 cells expressing endogenous IQGAP1 (green), IQGAP1$^{(-/-)}$ (blue), IQGAP1$^{(-/-)}$ transfected with Halo-IQGAP1 (pink), or IQGAP1$^{(-/-)}$ transfected with Halo-IQGAP1(CD), plated on micropatterns. Scale bars, 10 µm. **(B)** Quantification of mean fluorescence (pixel count) from cells in A. Dots represent values from individual cells (n = 20-41 cells). Error bars, SE. Statistics, ANOVA: a, significantly different from endogenous; b, significantly different from IQGAP1$^{(-/-)}$. Cells expressing IQGAP1(CD) plasmid were not significantly different than cells expressing IQGAP1 plasmid (p = 0.99). **(C)** Representative images of phalloidin-stained actin filaments from cells as in A. **(D)** Quantification and statistics of actin filament morphology as in B (n = 20-41 cells). Cells expressing IQGAP1(CD) plasmid were not significantly different than cells expressing IQGAP1 plasmid (p = 0.11). **(E)** Representative images from cells as in A 12 h post-wounding event. Scale bars, 200 µm. **(F)** Quantification of wound healing assays in E. Histograms represent means from n = 3-4 independent assays (dots). **(G)** Summary of IQGAP1 actin filament plus-end activities highlighting differences in on-rates and average dwell time. IQGAP1 displaces plus-end factors >18-fold more than the mDia1-CP decision complex. In cells, IQGAP1-filament capping activity may promote more turnover of molecules on filament plus-ends.

of cDNA, plasmid construction, subcloning, site-directed mutagenesis, and plasmid sequencing was performed by Genscript (Piscataway, NJ).

Plasmid Construction.

The coding sequence of full-length IQGAP1 (UniProt: G3V7Q7) was synthesized with a silent basepair substitution (c4485a) to remove a native KpnI restriction site and cloned into a modified pET23b vector (Pimm et al., 2022), flanked by AgeI and NotI sequences. IQGAP1 truncation mutants were subcloned into the same backbone or pET23b with a 5' SNAP-tag using the same restriction sites. Amino acid substitution mutations were generated in IQGAP1(745-1450) or the full-length protein using site directed mutagenesis to create: IQ1 (A754P, R757A, L760A), IQ1-2 (A754P, R757A, L760A, Q783A, W786A, R787A, K790A), IQ3 (H819A, R822A R826A), IQGAP1(CD) (C756A, C781A). To generate plasmids for mammalian cell expression, IQGAP1 and IQGAP1(CD) sequences were inserted into a pCDNA-Halo vector (Pimm et al., 2022) via KpnI and NotI restriction sites. 6×His-tagged mDia1(ΔDAD) (amino acids 1-1175) was synthesized and cloned into the pET23b vector flanked by AgeI and NotI restriction sites.

Protein purification, labeling, and handling.

All 6×His-tagged IQGAP1 proteins were expressed and purified using the same protocol as described for mDia1 constructs in Pimm et al 2022. Briefly, proteins were

expressed in Rosetta2(DE3) pRare2 cells (Millipore Sigma, Burlington, MA) and induced with 0.4 mM Isopropyl β-D-1-thiogalactopyranoside (IPTG) at 18 °C for 22 h. Cell pellets were resuspended in buffer (2× PBS (280 mM NaCl, 5 mM KCl, 20 mM sodium phosphate dibasic, 0.35 mM potassium phosphate monobasic, pH 8.0), 500 mM NaCl, 0.1% Triton-X 100, 14 mM β-mercaptoethanol (BME), 1 mg/mL DNase I, and 1× protease inhibitor cocktail (0.5 mg/mL leupeptin, 1000 U/mL aprotinin, 0.5 mg/mL pepstatin A, 0.5 mg/mL chymostatin, 0.5 mg/mL antipain)), and lysed with 1 mg/mL lysozyme for 20 min and probe sonication at 100 mW for 90 s. Clarified lysates were applied to cobalt affinity columns (Cytiva, Marlborough, MA), equilibrated in 1× PBS (pH 8.0), 500 mM NaCl, 0.1% Triton-X 100, 14 mM BME and eluted with a linear imidazole (pH 7.4) gradient (0-300 mM). The 6×His-SUMO-tag was cleaved using 5 μg/mL ULP1 protease and the final protein was gel filtered over a Superose 6 Increase (10/300) column (Cytiva) equilibrated with 1× PBS (pH 8.0), 150 mM NaCl, 14 mM BME. Proteins were labeled in 10-fold molar excess of SNAP-Surface dye (New England Biolabs, Ipswich, MA) in labeling buffer (1× PBS, 150 mM NaCl, 300 mM imidazole (pH 8.0), 0.1% Triton X-100, and 10 mM DTT) for 1 h, then the 6×His-SUMO-tag was cleaved, and gel filtered as above. Pooled fractions were concentrated, aliquoted, flash frozen, and stored at -80 °C until use.

GST-tagged IQGAP1 in pGEX-2T (AddGene: 30107) was expressed (as above) and induced for 18 h at 18 °C. Clarified lysate was batch bound to 1 mL of glutathione agarose beads for 2 h, washed with nine column volumes of 2× PBS (pH 8.0), 500 mM NaCl, 0.5 mM DTT, and eluted in 2× PBS, 150 mM NaCl, 5% glycerol, 0.1% Triton-X 100, 0.5 mM DTT, 15.3 mM glutathione. The GST-tag was removed with 44 μg/mL TEV protease, followed by gel filtration over a Superose 6 Increase (10/300) column (Cytiva) equilibrated with 1× PBS, 150 mM NaCl, 5% glycerol, 0.1% Triton-X 100, 0.5 mM DTT.

Purification of 6×His-mDia1(FH1-C) or 6×His-mDia1(ΔDAD) was conducted exactly as described for IQGAP1 or as we have purified previously (Liu et al., 2022; Pimm et al., 2022). Detailed purifications of untagged capping protein ($CP_{\alpha1\beta1}$; CP) in pET3d or 6×His-SNAP-CP in modified pET3d (Bombardier et al., 2015; Johnston et al., 2018; Soeno et al., 1998), profilin-1(Liu et al., 2022; Pimm et al., 2022), and labeled (OG-maleimide; Alexa-lysine) and unlabeled rabbit muscle actin (Cooper et al., 1984; Kuhn & Pollard, 2005; Pimm et al., 2022; Spudich & Watt, 1971) were described previously. Biotin-actin was purchased from Cytoskeleton, Inc (Denver, CO).

Protein concentrations were determined by densitometry of Coomassie gels compared to a BSA standard curve. Labeling efficiencies were calculated using spectroscopy and extinction coefficients: actinε_{290}, 25,974 M^{-1} cm^{-1}; Oregon Green (OG)ε_{496}, 70,000 M^{-1} cm^{-1}; Alexa-488ε_{495}, 73,000 M^{-1} cm^{-1}; SNAP-549ε_{554}, 140,300 M^{-1} cm^{-1}; Alexa-647ε_{650}, 203,000 M^{-1} cm^{-1}, and SNAP-649ε_{655}, 250,000 M^{-1} cm^{-1}. Correction factors used were: OG, 0.12; Alexa-488, 0.11; SNAP-549, 0.12; Alexa-647, 0.03; and SNAP-649, 0.03. The percent label for each SNAP-tagged protein is as follows: 549-SNAP-IQGAP1: 89%; 649-SNAP-IQGAP1: 87%; 488-SNAP-IQGAP(CD): 71%; 549-SNAP-mDia1(FH1-C): 57%; 549-SNAP-mDia1(ΔDAD): 66.5 or 70%; 549-SNAP-CP: 70%; and 647-SNAP-CP: 82%.

Total Internal Reflection Fluorescence (TIRF) microscopy and related analyses.

Coverslips were coated, imaging chambers were assembled, and TIRF microscopy was performed as previously described (Henty-Ridilla, 2022), with the following exceptions: reactions were conducted with 0.36% biotin-actin, at 20 °C, in: 20 mM imidazole (pH 7.4) 50 mM KCl, 1 mM $MgCl_2$, 1 mM EGTA, 0.2 mM ATP, 10 mM DTT, 40 mM glucose, and 0.25% methylcellulose (4000 cP). TIRF was performed using a DMi8 microscope equipped with 120-150 mW solid-state lasers, and a 100x Plan Apo 1.47 NA oil-immersion TIRF objective (Leica Microsystems, Wetzlar, Germany). Images were captured using an iXon Life 897 EMCCD camera (Andor; Belfast, Northern Ireland) with an 81.9 μm^2 field of view.

Images were processed in FIJI (Schindelin et al., 2012) with a 50-pixel rolling-ball radius background subtraction and 1.0-pixel Gaussian blur. Actin assembly experiments were visualized in 5 s intervals and dynamic parameters (i.e., nucleation and elongation rates) were determined as previously described (Henty-Ridilla, 2022). Nucleation was assessed 200 s (or 100 s in the supplement) following the addition of actin to each reaction. The durations of filament capping events were measured from actin filament length over time plots. Frequency distributions were displayed as best-fit values of a Gaussian distribution: $Y=(A)*(e^{(-0.5)*((x-|x|)/SD)2})$, where A is the amplitude of the peak and SD is the standard deviation of measured durations. For actin alone controls or capping deficient mutants, the data were not gaussian and best modeled as exponential decay: $Y= (Y_0-D_{max})*(e^{(-k*x)}+ D_{max})$, where D_{max} is the plateau and k is the exponential rate constant.

The oligomeric state of IQGAP1 or IQGAP1(CD) was measured from surface adsorbed 549-IQGAP1 or 488-IQGAP(CD) in TIRF buffer lacking glucose oxidase or catalase and recorded with continuous TIRF imaging at 75% laser power with no neutral density filter. Stepwise reductions in integrated fluorescence of individual molecules were scored by hand and compared to mathematical predictions (Breitsprecher et al., 2012).

Two-color TIRF movies of 647-actin seeds, 1 μM polymerizing actin (either 20% OG-label or 10% 488-label; 3.6 nM (0.36%) biotin-label), and 5 nM 549-IQGAP1 or 5 nM 488-IQGAP1(CD) were used to assess the localization to filament sides or ends over a 780 s period. Three-color TIRF movies of 1 μM actin (10% 488-label or 10% 647-label; 3.6 nM biotin-label), 5 nM 549-mDia1(ΔDAD) and 5 nM 649-IQGAP1, or 5 nM 549-mDia1 and 5 nM 488-

IQGAP1(CD) were similarly monitored over 1200 s. Colocalization was determined from room temperature TIRF reactions performed with 10 nM of each SNAP-labeled protein following a 10 min incubation period. Individual molecules were detected using the ComDet v.0.5.5 FIJI plugin (https://github.com/ekatrukha/ComDet), with a detection threshold set to 3 pixels and a maximum threshold set to 5 pixels. The ratio of overlapping signal was divided by the total limiting molecules (wavelength with the fewest total molecules) and multiplied by 100. Filament bundling was assessed by skewness parameter. Four-color TIRF movies were performed with 1 µM actin (30% 405-label and 3.6 nM (0.36%) biotin-label), 10 nM 488-SNAP-mDia1(ΔDAD), 10 nM 549-SNAP-CP, and 10 nM 649-SNAP-IQGAP1. Single-molecules and complexes were identified with the ComDet plugin, then fluorescence signal was monitored for each channel until molecule dissociation. Values were auto-binned and half-life was determined from best-fit values of an exponential decay.

Two-color actin experiments were performed by polymerizing 647-actin seeds (10% 647-label; 3.6 nM biotin-label) in TIRF chambers for 2-3 min. The chamber was washed thrice with TIRF buffer, and then the contents were replaced (leaving only 647-actin seeds) with a new reaction mix comprised of 0.5 µM actin (either 20% OG-label or 10% 488-label; 3.6 nM biotin-label) and buffer or buffer and unlabeled proteins. Bicolor filaments and 647-seeds were counted at 360 s and presented as the percent of 647-seeds lacking 488-actin (blocked ends) to the total number of 647-seeds per 81.9 µm^2.

Cell growth, screening, and fixation.

A pooled CRISPR knockout line and comparable wild-type NIH 3T3 cells expressing endogenous IQGAP1 were purchased from Synthego (Redwood City, CA). Cells were grown in DMEM (Gibco, Grand Island, NY) supplemented with 10% FBS (Genesee Scientific, San Diego, CA), 200 mM L-glutamine (Gibco), and 45 U/mL penicillin-streptomycin (Gibco). All cell lines were screened for mycoplasma at regular intervals by screening fixed cells for irregular DAPI stain. Clonal lines were produced via dilution by plating 0.5 cells per 48-well plate (Genesee Scientific) and visual confirmation of single-cell deposition. Wells containing cells were grown in conditioned media, grown to ~ 70% confluency, and screened for protein levels via Western blots with monoclonal mouse anti-IQGAP1 (1:1000; 610612, BD Biosciences, East Rutherford, NJ), polyclonal rabbit α-tubulin (1:2500; ab18251, Abcam Inc, Cambridge, United Kingdom), and appropriate secondary antibodies (1:5000 IR-dye-680 for IQGAP1 and IR-dye-800 for α-tubulin; LI-COR Biotechnology, Lincoln, NE). Blots were imaged with a LI-COR Odyssey Fc imaging system (LI-COR Biotechnology).

Cell morphology and wound healing assays.

M-FN coverslips (CYTOO Inc, Grenoble, France). After 30 min unattached cells were aspirated. IQGAP1$^{(-/-)}$ cells were transfected for 16 h with 500 ng empty vector, Halo-IQGAP1, or Halo-IQGAP1(CD) plasmids using Lipofectamine 3000 using manufacturer's instructions for 6-well plates. Cells were washed thrice in 1× PBS, washed into 0.3% glutaraldehyde and 0.25% Triton X-100 diluted in 1× PBS, and then fixed in 2% glutaraldehyde for 8 min. Autofluorescence was quenched with fresh 0.1%(w/v) sodium borohydride prepared in 1× PBS for 7 min at room temperature. Coverslips were washed twice with PBST (1× PBS and 0.1% Tween-20) supplemented with 1% BSA, blocked for 1 h at room temperature, and coverslips were stained with anti-α-tubulin (1:250; ab18251, Abcam) overnight at 4 °C. Cells were washed three times with PBST and incubated for 1 h with AlexaFluor-488 donkey anti-rabbit secondary (1:1000; A21206, Invitrogen, Waltham, MA), and AlexaFluor-568 phalloidin (1:500; Invitrogen). Coverslips were washed in 1× PBS and mounted in Aquamount (Andwin Scientific, Schaumburg, IL).

Coverslips were imaged by spinning disk confocal microscopy on an inverted Nikon Ti2-E microscope (SoRa; Nikon Instruments, Melville, NY) equipped with 488 nm and 561 nm wavelength lasers, a Plan Apo 60× 1.4 NA oil-immersion objective, a CSU-W1 imaging head (Yokogawa Instruments, Tokyo, Japan), a SoRa disk (Nikon Instruments, Melville, NY), and a Prime BSI sCMOS camera with a pixel size of 6.5 µm/pixel (Teledyne Photometrics, Tucson, AZ). Artificial intelligence denoise and 40 iterations of Richardson-Lucy deconvolution was applied to 7–10 µm Z-stacks acquired with Nikon Elements software. For morphology, and actin filament and microtubule arrays the total fluorescence signal (pixel count) threshold was set to saturated phalloidin-signal for morphology measurements, unsaturated phalloidin-signal for actin filaments, and unsaturated and tubulin labeled images. Images were converted to 8-bit grayscale, binarized, and measured as RawIntDen in Fiji software.

For wound-healing assays, 100,000 cells were transfected for 12 h in 6-well plates, replated following treatment with 100 µL 0.25% trypsin for 1 min, diluted with 1 mL of fresh media, and collected via centrifugation at 3000 x *g* for 3 min. Cells were gently resuspended in 200 µL of fresh media and transferred to each chamber (100 µL per well) of a polymer coated 2-well µ-dish (Ibidi, Martinsried, Germany). After 3 h incubation the chamber inserts were removed (time zero), the wound surface was washed thrice with warm Fluorobrite DMEM (Gibco) buffered with 10 mM HEPES (pH 7.4). Cells were visualized with CellMask Green or DeepRed plasma membrane stain (1:1000; Invitrogen) using the SoRa spinning disk described above, a Plan Apo 20× 0.75. NA air objective, and 3-4 concurrent fields of view spanning the wound gap. Plates were washed into standard media and returned to the incubation chamber between timepoints. Temperature was maintained during imaging with a heated stage insert (OKO labs, Pozzuoli, Italy). The image area occupied by cells was determined by tracing the area along the wound with the segmented line tool in FIJI. These outlines were used

to generate a binary mask of cell occupancy. Thus, percent closure is the ratio of cell occupancy at 12 h to occupancy at time zero.

Data analysis, statistics, and presentation.

GraphPad Prism 9 (version 9.5.0; GraphPad Software, San Diego, CA) was used to plot all data and perform statistical tests. The sample size, number of replicates, and statistical tests used for each experiment are in each figure legend. Individual data points are shown in each figure, histograms represent means (unless noted otherwise). Bars are standard error of mean. All ANOVA tests performed were one-way with Tukey post-hoc analysis. The threshold $p < 0.05$ was used to determine significance for comparisons throughout this work. Figures were made in Adobe Illustrator 2023 (version 27.1.1; Adobe, San Jose,CA).

Data availability.

Datasets for each figure have been uploaded and deposited, available here https://doi.org/10.5281/zenodo.7895840.

Supplemental information

Supplemental information includes 5 figures and 9 movies.

Acknowledgements

We are grateful to Marc Ridilla for helpful comments on this manuscript. We also thank J.P.B Pascal for showing us the Way. This work was supported by the National Institutes of Health (GM133485) to JLH-R.

Declaration of interests

The authors declare that they have no known competing financial or personal interests relevant to this work.

Author contributions

MLP, AGM, MAE, and JLH-R purified proteins. MLP and JLH-R designed experiments. MLP performed all TIRF experiments. MLP and BKH performed Western blots. AGM and JLH-R performed cell experiments. MLP and JLH-R made the figures and wrote the paper. All authors edited and read the submitted work.

References

1. Fujiwara, I., Remmert, K., Piszczek, G., and Hammer, J.A. (2014). Capping protein regulatory cycle driven by CARMIL and V-1 may promote actin network assembly at protruding edges. Proc. Natl. Acad. Sci. 111. 10.1073/pnas.1313738111.

2. Funk, J., Merino, F., Schaks, M., Rottner, K., Raunser, S., and Bieling, P. (2021). A barbed end interference mechanism reveals how capping protein promotes nucleation in branched actin networks. Nat. Commun. 12, 5329. 10.1038/s41467-021-25682-5.

3. Wear, M.A., Yamashita, A., Kim, K., Maéda, Y., and Cooper, J.A. (2003). How capping protein binds the barbed end of the actin filament. Curr. Biol. 13, 1531–1537. 10.1016/S0960-9822(03)00559-1.

4. Goode, B.L., and Eck, M.J. (2007). Mechanism and function of formins in the control of actin assembly. Annu. Rev. Biochem. 76, 593–627. 10.1146/annurev.biochem.75.103004.142647.

5. Kovar, D.R., Harris, E.S., Mahaffy, R., Higgs, H.N., and Pollard, T.D. (2006). Control of the assembly of ATP- and ADP-actin by formins and profilin. Cell 124, 423–435. 10.1016/j.cell.2005.11.038.

6. Rottner, K., Faix, J., Bogdan, S., Linder, S., and Kerkhoff, E. (2017). Actin assembly mechanisms at a glance. J. Cell Sci. 130, 3427–3435. 10.1242/jcs.206433.

7. Chesarone, M.A., DuPage, A.G., and Goode, B.L. (2010). Unleashing formins to remodel the actin and microtubule cytoskeletons. Nat. Rev. Mol. Cell Biol. 11, 62–74. 10.1038/nrm2816.

8. Breitsprecher, D., and Goode, B.L. (2013). Formins at a glance. J. Cell Sci. 126, 1–7. 10.1242/jcs.107250.

9. Zweifel, M.E., Sherer, L.A., Mahanta, B., and Courtemanche, N. (2021). Nucleation limits the lengths of actin filaments assembled by formin. Biophys. J. 120, 4442–4456. 10.1016/j.bpj.2021.09.003.

10. Breitsprecher, D., Jaiswal, R., Bombardier, J.P., Gould, C.J., Gelles, J., and Goode, B.L. (2012). Rocket launcher mechanism of collaborative actin assembly defined by single-molecule imaging. Science 336, 1164–1168. 10.1126/science.1218062.

11. Henty-Ridilla, J.L., Rankova, A., Eskin, J.A., Kenny, K., and Goode, B.L. (2016). Accelerated actin filament polymerization from microtubule plus ends. Science 352, 1004–1009. 10.1126/science.aaf1709.

12. Bradley, A.O., Vizcarra, C.L., Bailey, H.M., and Quinlan, M.E. (2020). Spire stimulates nucleation by Cappuccino and binds both ends of actin filaments. Mol. Biol. Cell 31, 273–286. 10.1091/mbc.E19-09-0550.

13. Montaville, P., Jégou, A., Pernier, J., Compper, C., Guichard, B., Mogessie, B., Schuh, M., Romet-Lemonne, G., and Carlier, M.-F. (2014). Spire and formin 2 synergize and antagonize in regulating actin assembly in meiosis by a ping-pong mechanism. PLoS Biol. 12, e1001795. 10.1371/journal.pbio.1001795.

14. Bosch, M., Le, K.H.D., Bugyi, B., Correia, J.J., Renault, L., and Carlier, M.-F. (2007). Analysis of the function of spire in actin assembly and its synergy with formin and profilin. Mol. Cell 28, 555–568. 10.1016/j.molcel.2007.09.018.

15. Hakala, M., Wioland, H., Tolonen, M., Kotila, T., Jegou, A., Romet-Lemonne, G., and Lappalainen, P. (2021). Twinfilin uncaps filament barbed ends to promote turnover of lamellipodial actin networks. Nat. Cell Biol. 23, 147–159. 10.1038/s41556-020-00629-y.

16. Mwangangi, D.M., Manser, E., and Robinson, R.C. (2021). The structure of the actin filament uncapping complex mediated by twinfilin. Sci. Adv. 7, eabd5271. 10.1126/sciadv.abd5271.

17. Stark, B.C., Lanier, M.H., and Cooper, J.A. (2017). CARMIL family proteins as multidomain regulators of actin-based motility. Mol. Biol. Cell 28, 1713–1723. 10.1091/mbc.E17-01-0019.

18. Wirshing, A.C.E., Rodriguez, S.G., and Goode, B.L. (2023). Evolutionary tuning of barbed end competition allows simultaneous construction of architecturally distinct actin structures. J. Cell Biol. 222, e202209105. 10.1083/jcb.202209105.

19. Ulrichs, H., Gaska, I., and Shekhar, S. (2023). Multicomponent regulation of actin barbed end assembly by twinfilin, formin and capping protein. 2023.04.24.538010. 10.1101/2023.04.24.538010.

20. Bombardier, J.P., Eskin, J.A., Jaiswal, R., Corrêa, I.R., Xu, M.-Q., Goode, B.L., and Gelles, J. (2015). Single-molecule visualization of a formin-capping protein 'decision complex' at the actin filament barbed end. Nat. Commun. 6, 8707. 10.1038/ncomms9707.

21. Shekhar, S., Kerleau, M., Kühn, S., Pernier, J., Romet-Lemonne, G., Jégou, A., and Carlier, M.-F. (2015). Formin and capping protein together embrace the actin filament in a ménage à trois. Nat. Commun. 6, 8730. 10.1038/ncomms9730.

22. Maufront, J., Guichard, B., Cao, L.-Y., Cicco, A.D., Jégou, A., Romet-Lemonne, G., and Bertin, A. (2022). Direct observation of the conformational states of formin mDia1 at actin filament barbed ends and along the filament. Mol. Biol. Cell 34, ar2. 10.1091/mbc.E22-10-0472.

23. Brown, M.D., and Sacks, D.B. (2006). IQGAP1 in cellular signaling: bridging the GAP. Trends Cell Biol. 16, 242–249. 10.1016/j.tcb.2006.03.002.

24. Hedman, A.C., Smith, J.M., and Sacks, D.B. (2015). The biology of IQGAP proteins: beyond the cytoskeleton. EMBO Rep. 16, 427–446. 10.15252/embr.201439834.

25. Shannon, K.B. (2012). IQGAP family members in yeast, Dictyostelium, and mammalian cells. Int. J. Cell Biol. 2012, 894817. 10.1155/2012/894817.

26. White, C.D., Erdemir, H.H., and Sacks, D.B. (2012). IQGAP1 and its binding proteins control diverse biological functions. Cell. Signal. 24, 826–834. 10.1016/j.cellsig.2011.12.005.

27. Brandt, D.T., Marion, S., Griffiths, G., Watanabe, T., Kaibuchi, K., and Grosse, R. (2007). Dia1 and IQGAP1 interact in cell migration and phagocytic cup formation. J. Cell Biol. 178, 193–200. 10.1083/jcb.200612071.

28. Cao, D., Su, Z., Wang, W., Wu, H., Liu, X., Akram, S., Qin, B., Zhou, J., Zhuang, X., Adams, G., et al. (2015). Signaling scaffold protein IQGAP1 interacts with microtubule plus-end tracking trotein SKAP and links dynamic microtubule plus-end to steer cell migration. J. Biol. Chem. 290, 23766–23780. 10.1074/jbc.M115.673517.

29. Hoeprich, G.J., Sinclair, A.N., Shekhar, S., and Goode, B.L. (2022). Single-molecule imaging of IQGAP1 regulating actin filament dynamics. Mol. Biol. Cell 33, ar2. 10.1091/mbc.E21-04-0211.

30. Liu, J., Kurella, V.B., LeCour, L., Vanagunas, T., and Worthylake, D.K. (2016). The IQGAP1 N-terminus forms dimers and the dimer interface is required for binding F-actin and Ca2+/calmodulin. Biochemistry 55, 6433–6444. 10.1021/acs.biochem.6b00745.

31. Ren, J.-G., Li, Z., Crimmins, D.L., and Sacks, D.B. (2005). Self-association of IQGAP1: characterization and functional sequelae*. J. Biol. Chem. 280, 34548–34557. 10.1074/jbc.M507321200.

32. Pelikan-Conchaudron, A., Le Clainche, C., Didry, D., and Carlier, M.-F. (2011). The IQGAP1 protein Is a calmodulin-regulated barbed end capper of actin filaments: possible implications in its function in cell migration. J. Biol. Chem. 286, 35119–35128. 10.1074/jbc.M111.258772.

33. Bashour, A.-M., Fullerton, A.T., Hart, M.J., and Bloom, G.S. (1997). IQGAP1, a Rac- and Cdc42-binding protein, directly binds and cross-links microfilaments. J. Cell Biol. 137, 1555–1566. 10.1083/jcb.137.7.1555.

34. Bartolini, F., Andres-Delgado, L., Qu, X., Nik, S., Ramalingam, N., Kremer, L., Alonso, M.A., and Gundersen, G.G. (2016). An mDia1-INF2 formin activation cascade facilitated by IQGAP1 regulates stable microtubules in migrating cells. Mol. Biol. Cell 27, 1797–1808. 10.1091/mbc.E15-07-0489.

35. Chen, A., Arora, P.D., Lai, C.C., Copeland, J.W., Moraes, T.F., McCulloch, C.A., Lavoie, B.D., and Wilde, A. (2020). The scaffold-protein IQGAP1 enhances and spatially restricts the actin-nucleating activity of Diaphanous-related formin 1 (DIAPH1). J. Biol. Chem., jbc.RA119.010476. 10.1074/jbc.RA119.010476.

36. Kuhn, J.R., and Pollard, T.D. (2005). Real-time measurements of actin filament polymerization by total internal reflection fluorescence microscopy. Biophys. J. 88, 1387–1402. 10.1529/biophysj.104.047399.

37. Liu, X., Pimm, M.L., Haarer, B., Brawner, A.T., and Henty-Ridilla, J.L. (2022). Biochemical characterization of actin assembly mechanisms with ALS-associated profilin variants. Eur. J. Cell Biol. 101, 151212. 10.1016/j.ejcb.2022.151212.

38. Pimm, M.L., Liu, X., Tuli, F., Heritz, J., Lojko, A., and Henty-Ridilla, J.L. (2022). Visualizing molecules of functional human profilin. eLife 11, e76485. 10.7554/eLife.76485.

39. Vizcarra, C.L., Bor, B., and Quinlan, M.E. (2014). The role of formin tails in actin nucleation, processive elongation, and filament bundling. J. Biol. Chem. 289, 30602–30613. 10.1074/jbc.M114.588368.

40. Romet-Lemonne, G., and Jégou, A. (2021). The dynamic instability of actin filament barbed ends. J. Cell Biol. 220, e202102020. 10.1083/jcb.202102020.

41. Shekhar, S., Pernier, J., and Carlier, M.-F. (2016). Regulators of actin filament barbed ends at a glance. J. Cell Sci. 129, 1085–1091. 10.1242/jcs.179994.

42. Courtemanche, N. (2018). Mechanisms of formin-mediated actin assembly and dynamics. Biophys. Rev. 10, 1553–1569. 10.1007/s12551-018-0468-6.

43. Fukata, M., Kuroda, S., Fujii, K., Nakamura, T., Shoji, I., Matsuura, Y., Okawa, K., Iwamatsu, A., Kikuchi, A., and Kaibuchi, K. (1997). Regulation of cross-linking of actin filament by IQGAP1, a target for Cdc42. J. Biol. Chem. 272, 29579–29583. 10.1074/jbc.272.47.29579.

44. Choi, S., Thapa, N., Hedman, A.C., Li, Z., Sacks, D.B., and Anderson, R.A. (2013). IQGAP1 is a novel phosphatidylinositol 4,5 bisphosphate effector in regulation of directional cell migration. EMBO J. 32, 2617–2630. 10.1038/emboj.2013.191.

45. Senger, F., Pitaval, A., Ennomani, H., Kurzawa, L., Blanchoin, L., and Théry, M. (2019). Spatial integration of mechanical forces by α-actinin establishes actin network symmetry. J. Cell Sci., jcs.236604. 10.1242/jcs.236604.

46. Efimova, N., Yang, C., Chia, J.X., Li, N., Lengner, C.J., Neufeld, K.L., and Svitkina, T.M. (2020). Branched actin networks are assembled on microtubules by adenomatous polyposis coli for targeted membrane protrusion. J. Cell Biol. 219, e202003091. 10.1083/jcb.202003091.

47. Pollard, T.D. (2016). Actin and actin-binding proteins. Cold Spring Harb. Perspect. Biol. 8. 10.1101/cshperspect.a018226.

48. Pimm, M.L., Hotaling, J., and Henty-Ridilla, J.L. (2020). Profilin choreographs actin and microtubules in cells and cancer. Int. Rev. Cell Mol. Biol., p. S1937644820300757. 10.1016/bs.ircmb.2020.05.005.

49. Skruber, K., Read, T.-A., and Vitriol, E.A. (2018). Reconsidering an active role for G-actin in cytoskeletal regulation. J. Cell Sci. 131. 10.1242/jcs.203760.

50. Gaillard, J., Ramabhadran, V., Neumanne, E., Gurel, P., Blanchoin, L., Vantard, M., and Higgs, H.N. (2011). Differential interactions of the formins INF2, mDia1, and mDia2 with microtubules. Mol. Biol. Cell 22, 4575–4587. 10.1091/mbc.e11-07-0616.

51. Jacquemet, G., Stubb, A., Saup, R., Miihkinen, M., Kremneva, E., Hamidi, H., and Ivaska, J. (2019). Filopodome mapping identifies p130Cas as a mechanosensitive regulator of filopodia stability. Curr. Biol. 29, 202-216.e7. 10.1016/j.cub.2018.11.053.

52. Samson, E.B., Tsao, D.S., Zimak, J., McLaughlin, R.T., Trenton, N.J., Mace, E.M., Orange, J.S., Schweikhard, V., and Diehl, M.R. (2017). The coordinating role of IQGAP1 in the regulation of local, endosome-specific actin networks. Biol. Open 6, 785–799. 10.1242/bio.022624.

53. Raz-Ben Aroush, D., Ofer, N., Abu-Shah, E., Allard, J., Krichevsky, O., Mogilner, A., and Keren, K. (2017). Actin turnover in lamellipodial fragments. Curr. Biol. 27, 2963-2973.e14. 10.1016/j.cub.2017.08.066.

54. Svitkina, T.M., Verkhovsky, A.B., McQuade, K.M., and Borisy, G.G. (1997). Analysis of the actin–myosin II system in fish epidermal keratocytes: mechanism of cell body translocation. J. Cell Biol. 139, 397–415. 10.1083/jcb.139.2.397.

55. Abraham, V.C., Krishnamurthi, V., Taylor, D.L., and Lanni, F. (1999). The actin-based nanomachine at the leading edge of migrating cells. Biophys. J. 77, 1721–1732.

56. Pollard, T.D., and Borisy, G.G. (2003). Cellular motility driven by assembly and disassembly of actin filaments. Cell 112, 453–465. 10.1016/S0092-8674(03)00120-X.

57. Chhabra, E.S., Ramabhadran, V., Gerber, S.A., and Higgs, H.N. (2009). INF2 is an endoplasmic reticulum-associated formin protein. J. Cell Sci. 122, 1430–1440. 10.1242/jcs.040691.

58. Mateer, S.C., Morris, L.E., Cromer, D.A., Benseñor, L.B., and Bloom, G.S. (2004). Actin filament binding by a monomeric IQGAP1 fragment with a single calponin homology domain. Cell Motil. 58, 231–241. 10.1002/cm.20013.

59. Johnston, A.B., Hilton, D.M., McConnell, P., Johnson, B., Harris, M.T., Simone, A., Amarasinghe, G.K., Cooper, J.A., and Goode, B.L. (2018). A novel mode of capping protein-regulation by twinfilin. eLife 7, e41313. 10.7554/eLife.41313.

60. Zhang, M., Li, Z., Jang, H., Hedman, A.C., Sacks, D.B., and Nussinov, R. (2019). Ca 2+-dependent switch of calmodulin interaction mode with tandem IQ motifs in the scaffolding protein IQGAP1. Biochemistry 58, 4903–4911. 10.1021/acs.biochem.9b00854.

61. Soeno, Y., Abe, H., Kimura, S., Maruyama, K., and Obinata, T. (1998). Generation of functional β-actinin (CapZ) in an E. coli expression system. J. Muscle Res. Cell Motil. 19, 639–646. 10.1023/A:1005329114263.

62. Spudich, J.A., and Watt, S. (1971). The regulation of rabbit skeletal muscle contraction: I. biochemical studies of the interaction of the tropomyosin-troponin complex with actin and the proteolytic fragments of myosin. J. Biol. Chem. 246, 4866–4871. 10.1016/S0021-9258(18)62016-2.

63. Cooper, J.A., Blum, J.D., and Pollard, T.D. (1984). Acanthamoeba castellanii capping protein: properties, mechanism of action, immunologic cross-reactivity, and localization. J. Cell Biol. 99, 217–225. 10.1083/jcb.99.1.217.

64. Henty-Ridilla, J.L. (2022). Visualizing actin and microtubule coupling dynamics in vitro by total internal reflection fluorescence (TIRF) microscopy. J. Vis. Exp., 64074. 10.3791/64074.

65. Schindelin, J., Arganda-Carreras, I., Frise, E., Kaynig, V., Longair, M., Pietzsch, T., Preibisch, S., Rueden, C., Saalfeld, S., Schmid, B., et al. (2012). Fiji: an open-source platform for biological-image analysis. Nat. Methods 9, 676–682. 10.1038/nmeth.2019.

Supplemental Information

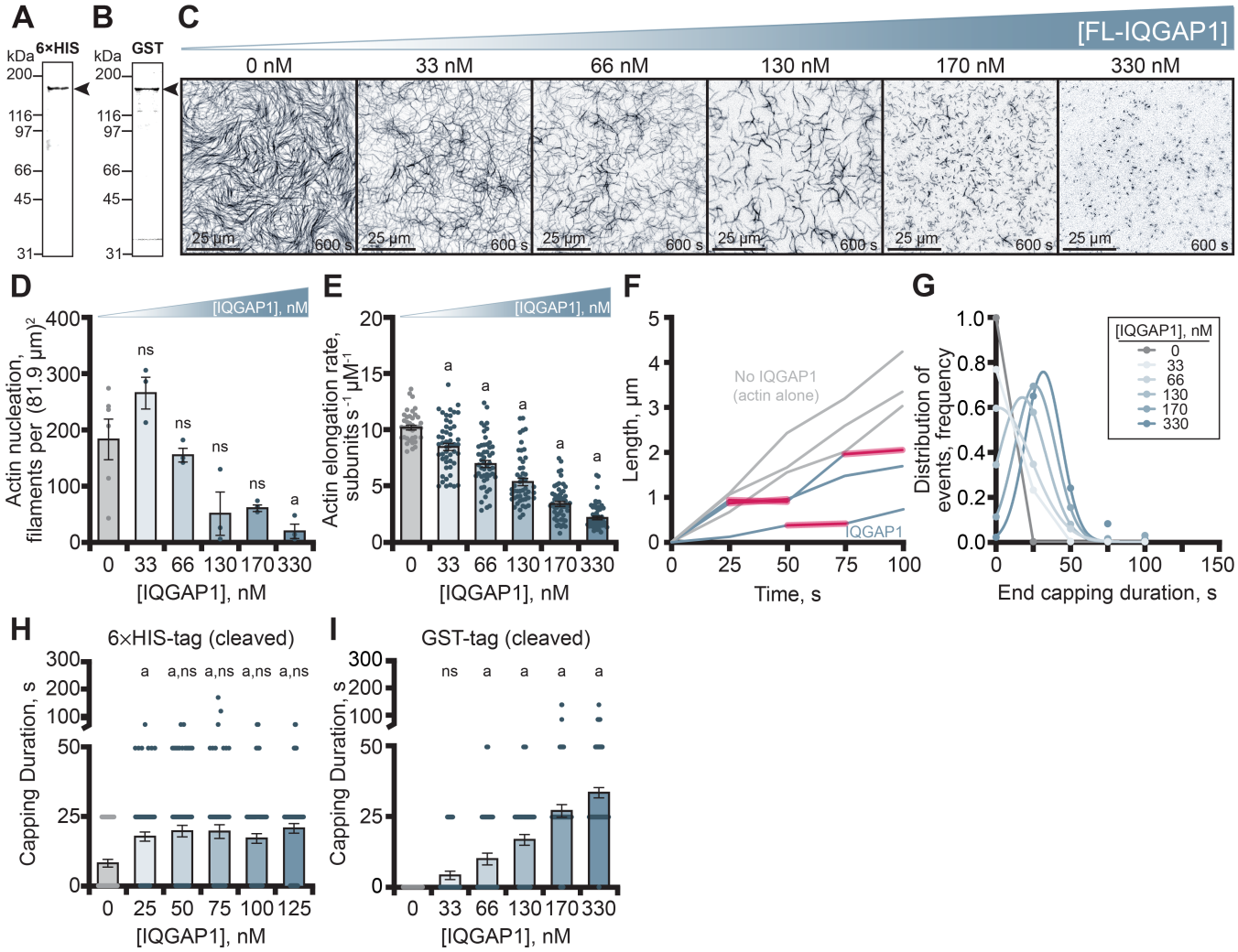

Supplemental Figure 1. Evaluation of IQGAP1 activities after GST affinity purification. SDS-PAGE gels of IQGAP1 purified by **(A)** 6×His or **(B)** GST affinity. **(C)** TIRF microscopy images from reactions containing 1 µM actin monomers (20% OG-label) and concentrations of IQGAP1. Scale bars, 25 µm. **(D)** Actin filament nucleation 100 s after initiation from reactions as in C (n = 3 fields of view; dots). Error bars indicate SE. Statistics, ANOVA: a, significantly different from actin control (0 nM IQGAP1); ns, not different from control. **(E)** Actin filament elongation rates from TIRF reactions as in C (n = 30-50 filaments per condition; pooled from 3-6 different trials). Statistics as in D. **(F)** Example length over time plots from reactions containing actin (grey) or actin and 66 nM IQGAP1 (teal). Red shading denotes length of pausing events. **(G)** Duration of IQGAP1 capping events from frequency distribution plots from F (n = 38-50 filaments, and 12-98 pause events per condition, 237 pauses measured). The mean duration of individual capping events was 19.9 s in the presence of IQGAP1 (regardless of concentration). Distribution of the duration of IQGAP1 capping events with protein purified by **(H)** 6×His (n = 75 filaments, and 31-70 pause events per condition, 331 total pauses measured; individual data points for plots in Figure 1G) or **(I)** GST affinity (n = as in G). Statistics as in D.

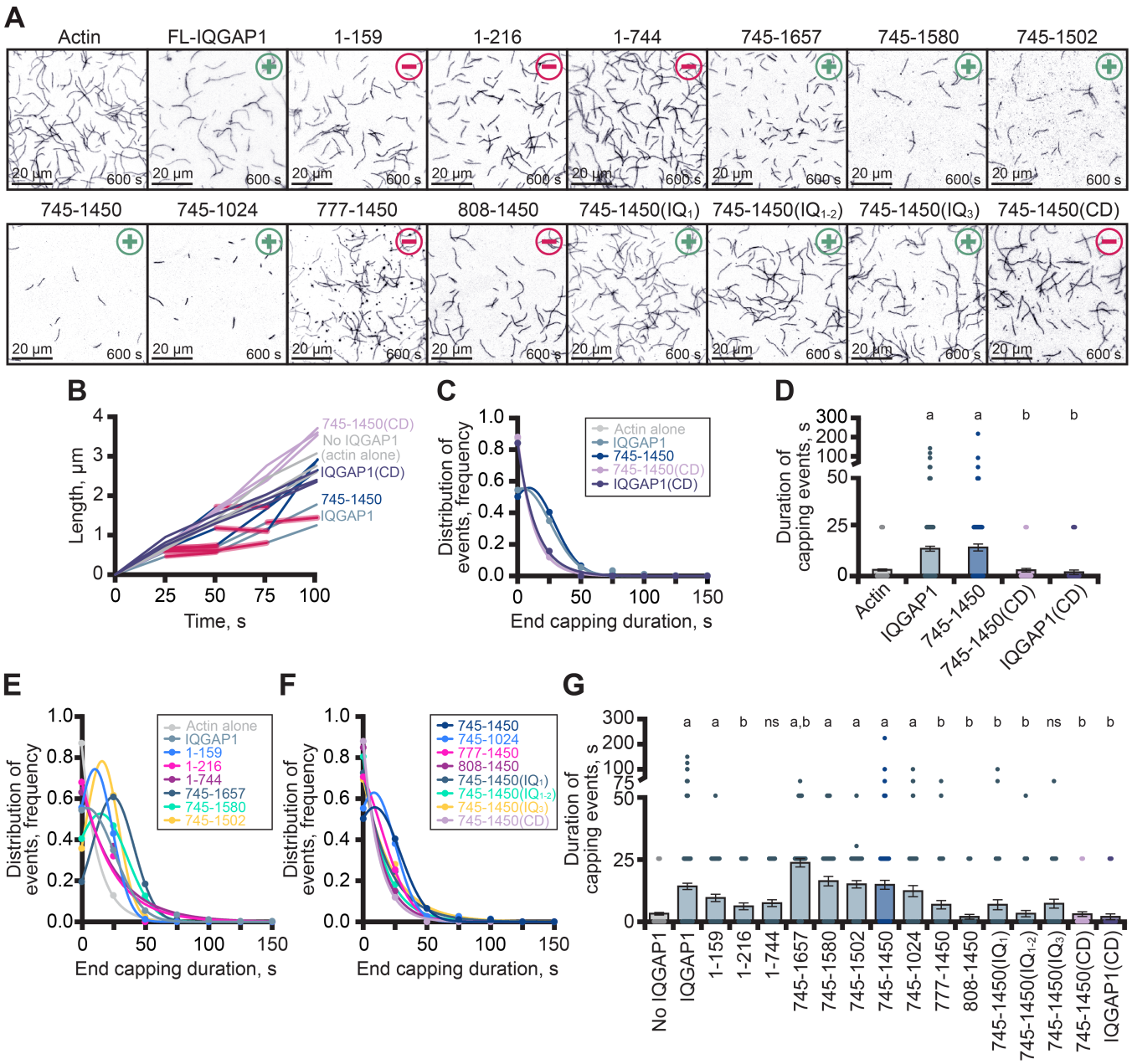

Supplemental Figure 2. Regions necessary for IQGAP1 capping activity. **(A)** Images from TIRF assays containing 1 µM actin (20% OG-label) or actin and 75 nM IQGAP1 proteins that cap (+) and fail to cap (–) actin filaments. Scale bars, 20 µm. **(B)** Filament traces, **(C)** frequency plots, and **(D)** distribution of individual capping event durations used in C (n = 256 filaments, 159 events per condition). Error bars indicate SE. Statistics, ANOVA: a, significantly different from no IQGAP1 control; b, significantly different from IQGAP1; ns, not different from control. **(E-F)** Frequency plots for various IQGAP1 proteins and **(G)** distribution of the capping event durations used for E-F (n = 75-324 filaments, 91-159 events for capping proficient constructs; 9-12 events for deficient constructs). Statistics as in D. IQGAP1(CD) or 745-1450(CD) do not cap actin filaments. For direct comparisons, values in B-C are replotted from Figure 2D-E. Values in D are replotted in G.

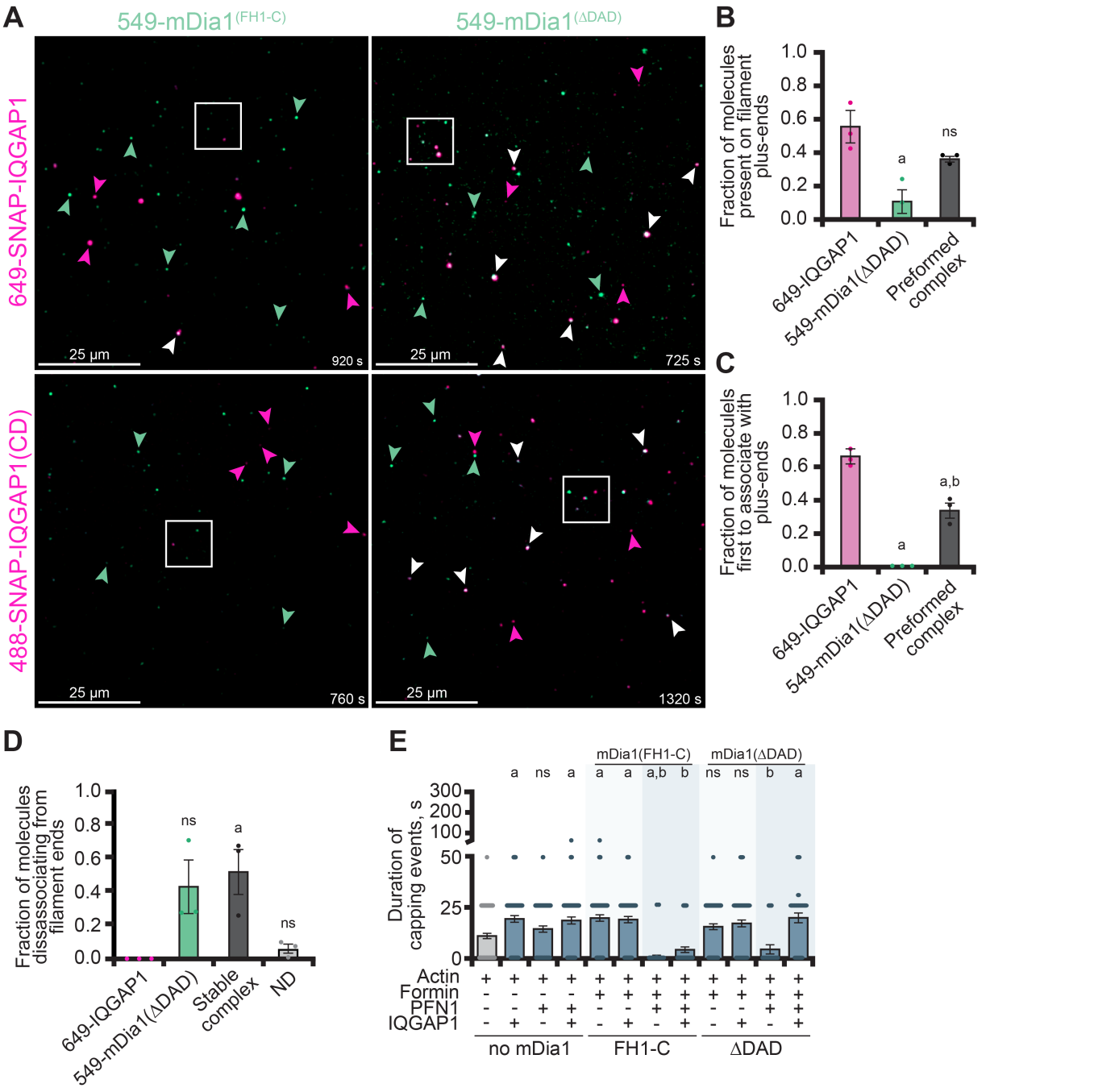

Supplemental Figure 3. Formation of IQGAP1-mDia1 complexes. **(A)** Single-molecule colocalization of 10 nM 549-mDia1 constructs with 10 nM 649-IQGAP1 or 10 nM 488-IQGAP1(CD) by TIRF. Arrows highlight examples of SNAP-IQGAP1 (pink), SNAP-mDia1 (green) or colocalized molecules (white). White box shown in Figure 4B. Scale bars, 25 μm. **(B)** Fraction of IQGAP1, mDia1(ΔDAD) or IQGAP1-mDia1(ΔDAD) complexes observed on actin filament plus-ends from reactions containing: 1 μM actin (10% Alexa-488 label), 10 nM 649-IQGAP1, and 10 nM 549-mDia1(ΔDAD) (n = 54 occupied ends from 111 total filaments, n = 3 movies). Error bars indicate SE. Statistics, ANOVA: a, significantly different from IQGAP1; b, significantly different from formin. **(C)** Molecule to first associate with actin filament plus-ends from reactions in B (n = 30 observations per condition). **(D)** Fraction of dissociation events recorded from reactions in B (n = 30 observations per condition from movies in B. Statistics as in B. Not determined, fraction of molecules not dissociated at the end of the observation period. **(E)** Distribution of capping event durations determined from actin filaments measured in Figure 4F. Dots represent individual filament pausing events measured (n = 24-105 per condition, pooled from at least 3 independent trials). Statistics, ANOVA: a, different from actin alone or formin controls; b, different from reactions containing formin and PFN1.

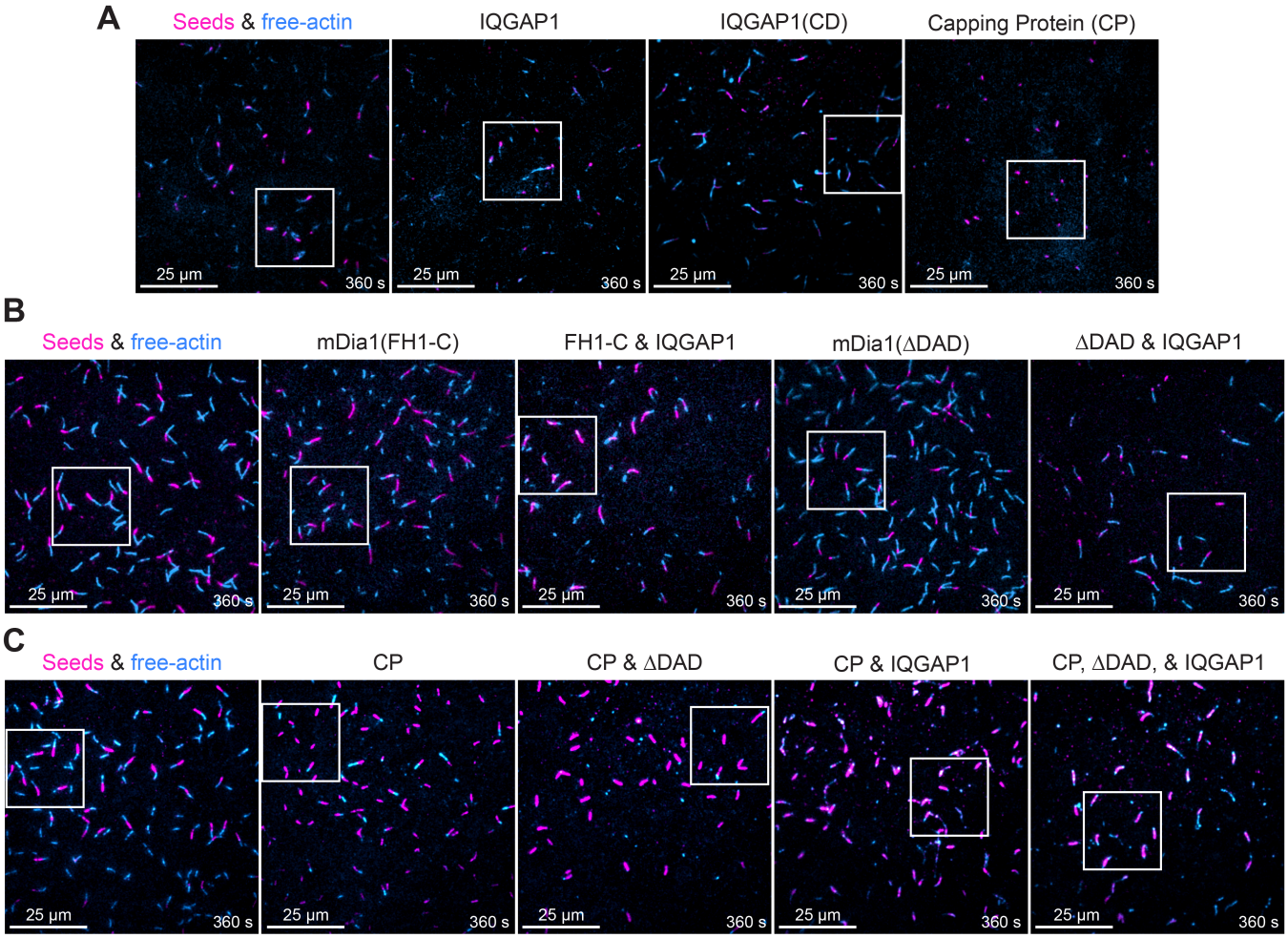

D

Plus-end Bound Molecules	Associating Molecules	K_{on} (s^{-1} μM^{-1})	K_{off} (ms^{-1})	Plus-end Dwell Time (s)	Fold Difference to CP	Fold Diffence to mDia1	n
-	IQGAP1[1]	1.6-3.2	40	25	-80	-200	-
-	mDia1[2]	29.1	0.1	119-5000	2.5	-	-
-	CP[3]	7.3	0.6	~2000	-	-2.5	-
mDia1	IQGAP1[4]	ND	ND	ND	-	-	-
mDia1	CP[5]	0.08-0.2	1800	161-714	-2.8	-7.0	-
CP	IQGAP1	0.02	5.6	180	-11.1	-27.7	3
CP	mDia1[2]	1.6	4.2-6.3	158-238	-8.4	-21	-
IQGAP1	mDia1	2.71	46	22	-90	-227.3	30
IQGAP1	CP	0.08	4	250	-8	-20	7
Formin-IQGAP1	CP	0.278	13.9	72	-27.8	-69.4	5
Decision Complex	-	ND	2.0	493	-4.1	-10.1	20
More Complex Decisions	**-**	**ND**	**37**	**27**	**-74.1**	**-185.2**	**21**

[1]Similar to values determined in Hoperich et al. 2022 and Pelikan-Conchaudron et al. 2011.
[2]Values determined: Bombardier et al. 2015, Shekhar et al. 2015, and Cao et al 2018. The longest value was used for comparison.
[3]Values determined in: Fujiwara et al. 2014 and Funk et al. 2021. The longest value was used for comparison.
[4]Values determined for IQGAP1(CHD) in Brandt et al. 2007 and Chen et al. 2020. Values do not consider plus-end binding.
[5]Values determined: Bombardier et al. 2015 and Shekhar et al. 2015.

Supplemental Figure 4. Capping Protein is less efficient at blocking actin assembly in the presence of IQGAP1. TIRF images of bicolor actin assays containing: 647-actin filament seeds, 0.5 μM actin monomers (20% OG (top row only) or 10% 488-Alexa label) and **(A)** buffer (control), 250 nM IQGAP1, 250 nM IQGAP1(CD), or 10 nM Capping Protein (CP); **(B)** buffer, 10 nM mDia1 protein, or 250 nM IQGAP1 and 10 nM mDia1 protein; **(C)** buffer, CP, CP and mDia1(ΔDAD), CP and IQGAP1, or CP, mDia1(ΔDAD), and IQGAP1. White box shown in Figure 5. Scale bars, 25 μm. **(D)** Summary table of actin filament plus-end dynamics with IQGAP1, mDia1, CP, or various complexes determined from four-color TIRF assays in Figure 6A.

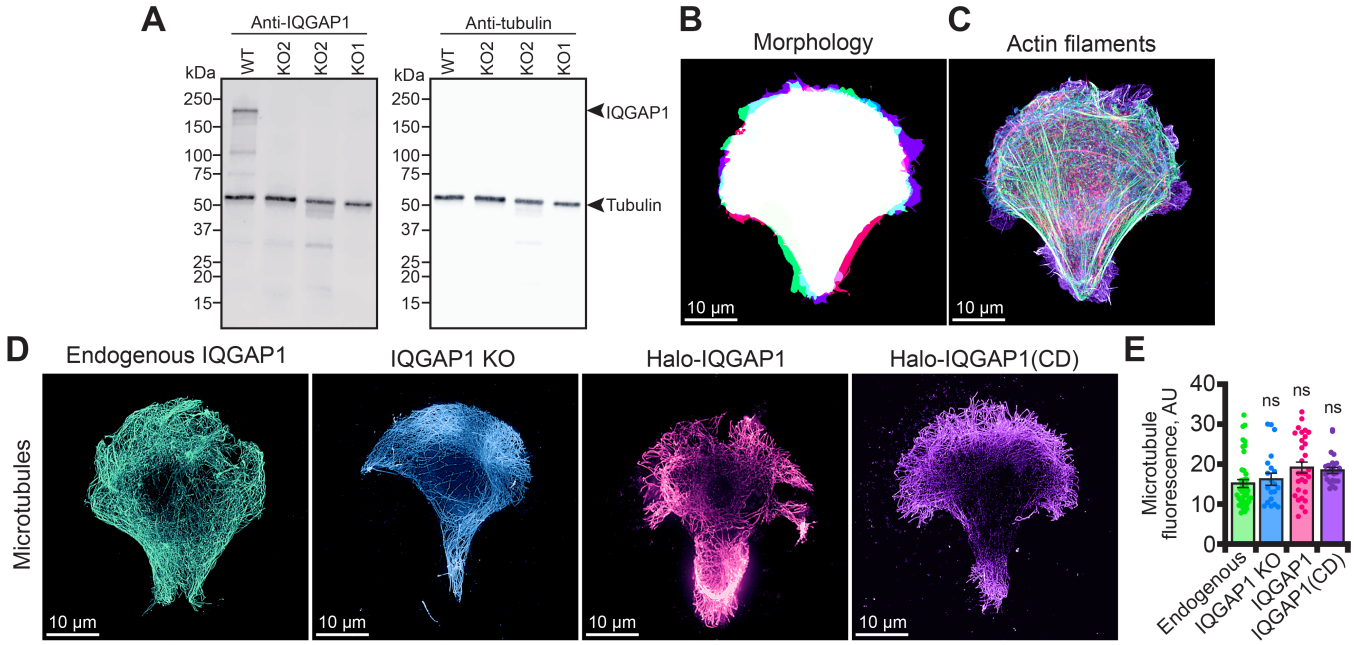

Supplemental Figure 5. IQGAP1 is required for normal morphology and cytoskeletal organization in 3T3 cells. **(A)** Representative full blots confirming knockout of IQGAP1 (n = 3 blots). Extracts prepared from endogenous IQGAP1$^{(+/+)}$ or two clonal IQGAP1$^{(-/-)}$ knockout cell lines. Blot was probed with (left) monoclonal mouse anti-IQGAP1 (1:1000; BD610612) and (right) polyclonal rabbit α-tubulin (1:2500; ab18251), and appropriate secondary antibodies (1:5000 IR-dye-680 for IQGAP1 and IR-dye-800 for α-tubulin). Maximum intensity overlays of 3T3 cell **(B)** cell morphology or **(C)** phalloidin-stained actin filaments expressing IQGAP1 (green), IQGAP1$^{(-/-)}$ (blue), IQGAP1$^{(-/-)}$ transfected with Halo-IQGAP1 (pink), or IQGAP1$^{(-/-)}$ transfected with Halo-IQGAP1(CD). Images associated with Figure 7. Scale bars, 10 µm. **(D)** Maximum intensity images of microtubules and **(E)** associated quantification of fluorescence. Color code as in B-C. Statistics, ANOVA: ns, not significant.

Movie Legends

Movie 1 (associated with Figure 1B). Polymerizing actin filaments in the absence or presence of IQGAP1. Reactions contain: 1 μM actin monomers (20% OG labeled) and concentrations of IQGAP1. Playback, 10 FPS. Scale bars, 20 μm.

Movie 2 (associated with Figure S1C). Polymerizing actin filaments in the absence or presence of IQGAP1 purified by GST affinity. Reactions contain: 1 μM actin monomers (20% OG labeled) and concentrations of IQGAP1 (purified by GST affinity). Playback, 10 FPS. Scale bars, 20 μm.

Movie 3 (associated with Figure 1E). Example of IQGAP1-mediated actin filament capping. Reactions contain: 1 μM actin monomers (20% OG labeled) and 75 nM IQGAP1. Arrows depict growth (green) or pausing (red). Playback, 10 FPS. Scale bars, 5 μm.

Movie 4 (associated with Figure 2B). IQGAP1(CD) does not cap actin filaments. Reactions contain: 1 μM actin monomers (20% OG labeled) or actin and 75 nM IQGAP1 protein. Playback, 10 FPS. Scale bars, 10 μm.

Movie 5 (associated with Figure S2A). Capping activity of IQGAP1 truncations and mutations. Reactions contain: 1 μM actin monomers (20% OG labeled) or actin and 75 nM IQGAP1 protein. Playback, 10 FPS. Scale bars, 10 μm.

Movie 6 (associated with Figure 3D). SNAP-IQGAP1 binds actin filament sides and plus-ends while SNAP-IQGAP1(CD) only binds filament sides. Left: Reactions contain: 1 μM actin monomers (20% OG labeled) and 5 nM 649-SNAP-IQGAP1. Panels show individual wavelengths and merge. Arrows indicate free (blue) or IQGAP1-capped (pink) plus-ends. Playback, 10 FPS. Scale bars, 5 μm. Right: Reactions contain: 1 μM actin monomers (10% Alexa-647 labeled) and 5 nM 488-SNAP-IQGAP1(CD). Panels show individual wavelengths and merge. Arrows indicate free plus-ends (pink) or IQGAP1 molecules on filament sides (blue). Playback, 10 FPS. Scale bars, 5 μm.

Movie 7 (associated with 4D). IQGAP1-mDia1 complexes stall plus-end growth and IQGAP1(CD) does not influence plus end dynamics. Top: Reactions contain: 1 μM actin monomers (10% Alexa-488 labeled) and 5 nM 649-SNAP-IQGAP1 and 549-SNAP-mDia1(ΔDAD) which retains the IQGAP1 binding site. Panels show individual wavelengths and merge. Actin filament growth resumes once IQGAP1 leaves the complex. Arrows indicate free plus-ends (blue), individual molecules of IQGAP1 (pink) or formin (green), or IQGAP1-CP complexes (white). Playback, 10 FPS. Scale bars, 5 μm. Bottom: Reactions contain: 1 μM actin monomers (10% Alexa-647 labeled) and 5 nM 488-SNAP-IQGAP1(CD) and 549-SNAP-mDia1(ΔDAD). Panels show individual wavelengths and merge. Arrows indicate free plus-ends (blue), individual molecules of IQGAP1(CD) (pink) or formin (green). Playback, 10 FPS. Scale bars, 5 μm.

Movie 8 (associated with 5B, 5D, and 5F). IQGAP1 caps actin filaments and blocks mDia1(ΔDAD)-mediated filament elongation more than mDia1(FH1-C). Top: Reactions contain: 647-actin seeds polymerized from 1 μM actin monomers, 0.5 μM actin monomers (20% OG label) and buffer (control), 250 nM IQGAP1, 250 nM IQGAP1(CD), or 10 nM Capping Protein (CP). Arrows highlight growing (blue) or capped (pink) filaments. Playback, 10 FPS. Scale bars, 10 μm. Middle: Reactions contain: 647-actin seeds polymerized from 1 μM actin monomers, 0.5 μM actin monomers (10% Alexa-488 label) and buffer (control), 10 nM mDia1(FH1-C) which does not bind IQGAP1, 250 nM IQGAP1 and mDia1(FH1-C), 10 nM mDia1(ΔDAD) which binds IQGAP1, or 250 nM IQGAP1 and mDia1(ΔDAD). Arrows highlight growing (blue) or capped (pink) filaments. Playback, 10 FPS. Scale bars, 10 μm. Bottom: Reactions contain: 647-actin seeds polymerized from 1 μM actin monomers, 0.5 μM actin monomers (10% Alexa-488 label) and buffer (control), 10 nM Capping Protein (CP), 10 nM CP and 10 nM mDia1(ΔDAD), 10 nM CP and 250 nM IQGAP1, or CP, mDia1(ΔDAD) and IQGAP1. Arrows highlight growing (blue) or capped (pink) filaments. Playback, 10 FPS. Scale bars, 10 μm.

Movie 9 (associated with 6A). IQGAP1 skews decision complexes in favor of filament growth. Reactions contain: 1 μM actin monomers (30% 405-label), 10 nM 488-mDia1(ΔDAD), 10 nM 549-Capping Protein (CP) and 10 nM 649-IQGAP1. Arrows highlight molecules/complex oligomerization at plus-ends (purple), formin (green), CP (yellow), or IQGAP1 (pink). Playback, 15 FPS. Scale bar, 2 μm.